TÉCNICO LISBOA

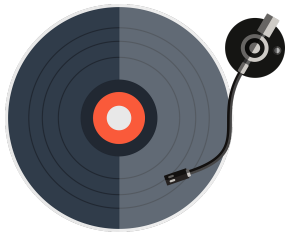

Accretion disks around compact objects

Author:
Pedro Alexandre Palma Piçarra

Supervisor:
Vítor Manuel dos Santos Cardoso

Research work performed at

CENTRA - GRIT

to obtain a Master of Science Degree in

Physics Engineering

Examination Committee

Chairperson:	Ilídio Pereira Lopes
Supervisor:	Vítor Manuel dos Santos Cardoso
Member of the Committee:	David Mathew Hilditch
	Richard Pires Brito

Outubro & 2022

"L'amor che move il sole e l'altre stelle."

Dante, Paradiso XXXIII, v. 145

Ao Silva.

Acknowledgments

My first acknowledgment belongs to my supervisor, prof. Vitor Cardoso, for guiding me through the intricate paths of General Relativity. Thank you for having me as one of your students and for all the fruitful discussions we shared.

I would not have been allowed to pursue my dream of studying physics if it was not for the caring support of my grandparents. I keenly thank them for that. I also want to thank my parents for their persistent guidance and unconditional support.

I am now the proud owner of a 1/3 of a microwave, I owe Daniel and Mariana for that.

I want to thank David, Ivo and Ricardo for all the moments of bursting laughter we shared while in desperation to finish a report. I am sure I would never be able to complete this journey without your friendship.

I want to thank Tomás Cabrito for the memes and for all the passionate conversations. I am grateful to Simplício for reminding me of the pleasure of discussing physics. I also want to thank Anita, Braga and Tomás Lopes for their incredible support while writing this thesis.

For all the coffee and infinite patience, I thank Caturra. I also want to thank Madalena for always being upset with me through these years.

Resumo

Um dos maiores desafios que enfrentamos em astrofísica é estudar buracos negros e compreender de que forma a relatividade geral os decreve adequadamente. Acredita-se que os candidatos a buracos negros sejam bem descritos pela solução de Kerr. Contudo, a evidenciência de matéria escura e o comportamento anómalo da gravidade no interior do horizonte de eventos levam-nos a considerar outras soluções de espaço-tempo conhecidas como *black hole mimickers*. Algumas teorias sugerem que campos escalares bosónicos podem formar soluções compatas estáveis, dificeis de distinguir observavelmente de buracos negros, intituladas de estrelas dea bosões. Neste projeto, consideramos o seu limite para campos fracos, isto é, campos escalares muito leves ($\sim 10^{-17} eV$) acoplados de forma fraca com a gravidade, conhecido como estrela de bosões Newtoniana. O nosso objetivo é estudar se estas soluções podem reproduzir a acreção de um buraco negro de Kerr, sendo potenciais *black hole mimickers*. Aplicando o modelo de Novikov-Thorne, descrevemos a acreção de um disco estacionário, fino, e opticamente denso. Comparamos o fluxo eletromagnético de discos em torno de buracos negros e de estrelas de bosões newtonianas, identificando assinaturas sobre a natureza do objecto acretante. Encontramos um espaço de parâmetros de massa e rotação do buraco negro tal que a luminosidade bolométrica dos discos é a mesma. Discutimos como o espectro de emissão dos discos na banda mais energética do ultravioleta pode ser usado para diferenciar as duas soluções de espaço-tempo. Por fim, verificamos se estrelas de bosões newtonianas descrevem as luminosidades de alguns centros galáticos ativos. Concluimos que estes que são consistentes com soluções compactas de campos escalares leves ($\sim 10^{-16} - 10^{-19} eV$).

Palavras-chave: Buraco Negro de Kerr; Estrela de bosões; disco de acreção; modelo de Novikov-Thorne

Abstract

A major challenge we face in astrophysics is to study black holes and understand how good a description general relativity is for them. Black hole candidates are believed to be well described by the Kerr solution. However, the existence of dark matter evidence and the pathological behaviour of gravity inside the horizon motivate the search for other spacetime solutions, known as black hole mimickers. Some theories suggest that scalar boson fields could form stable self-gravitating solutions, hard to distinguish through observations from black holes, known as boson stars. In this work, we take their weak field limit, consisting of very light fields ($\sim 10^{-17} eV$) weakly coupled to gravity, known as Newtonian boson stars. Our goal is to study if these solutions could mimic the accretion of a Kerr black hole and potentially be considered black hole mimickers. Working with the Novikov-Thorne model, we describe the accretion dynamics for steady geometrically thin and optically thick accretion disks. We compare the thermal flux profiles of disks around black holes and Newtonian boson stars, identifying signatures relating to the nature of the accreting compact object. A parameter space of mass and Black Hole spin is found such that the disks have the same bolometric luminosities. We discuss how the emission spectra of the disk for the high UV band can be considered to discern the two spacetime solutions. In conclusion, we check if Newtonian boson stars describe active galaxy nuclei luminosity observables and find them consistent with self-gravitating light scalar fields ($\sim 10^{-16} - 10^{-19} eV$).

Keywords: Kerr black hole; Boson star; Accretion disk; Novikov-Thorne model

Contents

List of Figures

Glossary

AD Accretion disk.

BH Black Hole.

BS Boson Star.

DM Dark Matter.

GR General Relativity.

NBS Newtonian Boson Star.

Chapter 1

Introduction

1.1 General relativity

The story of a mathematical description of gravity starts with the publication of *Principia* [4] in 1687 where Newton presented his universal law of gravitation. In Newtonian physics, gravity is an attractive radial force $\vec{F}$ acting on massive bodies, whose strength depends on their masses, on the inverse of the square of the distance r between them and on a gravitational constant G

$$\vec{F} = G\frac{Mm}{r^2}\vec{e}_r, \tag{1.1}$$

where m and M are the bodies masses and $\vec{e}_r$ is the radial unit vector.

The theory is remarkably accurate for small energies, masses and velocities. In fact, the theoretical prediction of the existence of Neptune by John Adams and Urbain Le Verrier and the moon landing in 1969 were achieved using Newtonian gravity only.

However, there were some astronomical observations such as the precession of the perihelion of Mercury which could not be explained under Newtonian gravity. Besides, in 1905 Einstein published the theory of special relativity [5] postulating that no physical effect can propagate faster than the speed of light. This was inconsistent with Newton's instantaneous theory, motivating the search for a covariant description of gravity. In Newtonian physics, the Poisson equation $\nabla^2\Phi = 4\pi G\rho$ relates the gravitational potential Φ with the matter density ρ which is originating it. When Einstein came up with his famous relation between rest mass m and energy $E = mc^2$ it became clear that energy alone could also be a source of gravity and the equations should account for such effect.

In 1916, Einstein published the theory of general relativity (GR) [6]. GR theory asserts that space and time are not independent concepts but a continuum: spacetime, i.e., a 4-dimensional manifold with a tangent space defined everywhere where special relativity holds locally. Spacetime is described by a metric field $g_{\mu\nu}$ which defines length and time, encoding the information of the gravitational potential. The Einstein field equations of GR consist of 10 nonlinear differential equations relating the universe matter content, encoded in the stress-energy tensor $T_{\mu\nu}$, with spacetime curvature, encoded in the Einstein tensor $G_{\mu\nu}$:

$$G_{\mu\nu} + \Lambda g_{\mu\nu} = \frac{8\pi G}{c^4} T_{\mu\nu}, \tag{1.2}$$

where Λ is the cosmological constant. According to GR, gravity is the result of spacetime curvature caused by the universe energy-matter content. However, the Einstein field equations alone are not sufficient to describe the whole picture. For this, we must include the geodesic equation (1.3), which explains how spacetime curvature affects matter dynamics:

$$\frac{d^2x^\mu}{ds^2} + \Gamma^\mu{}_{\alpha\beta} \frac{dx^\alpha}{ds} \frac{dx^\beta}{ds} = 0, \tag{1.3}$$

where s is any affine parameter along the worldline and $\Gamma^\mu{}_{\alpha\beta}$ are the Christoffel symbols. On one hand, the energy-matter content of the universe curves spacetime, on the other hand, the spacetime curvature itself affects the dynamics of the universe's energy-matter content.

1.2 Black holes

The idea of an astrophysical object so massive that not even light could escape from it - a dark star - was originally proposed by John Michell [7] in 1783. Using Newtonian physics, and considering light to be made out of massive particles travelling with a velocity c, he derived the radius R_S of such objects as a function of their mass M, coincidentally obtaining the Schwarzschild radius:

$$R_S = \frac{2GM}{c^2}. \tag{1.4}$$

However dark, these objects would still affect the motion of neighbouring bodies, and their existence could still be indirectly inferred. Despite being mentioned in the work of many remarkable physicists like Laplace, the idea of dark stars was discarded for centuries for the lacking of a theory about the gravitational influence on massless waves, which replaced the Newtonian corpuscular theory of light.

GR was able to provide a consistent explanation about the gravitational effect on light: photons follow spacetime null geodesics, resulting in light bending close to massive bodies. The more massive an object is, the more bent the photon trajectory will be. Thus, there exists a mass beyond which the photon path is closed upon the surface of the object and light can not escape from it.

The understanding of what could be at the origin of these dark stars would come much later, relying on the developments in stellar evolution. A star lives as long as nuclear reactions occur at its core, forming new elements and releasing a huge amount of energy. This energy exerts pressure on matter balancing the gravitational pull and preventing the star from collapsing. Once a star drains out of fusion fuel, the gravitational pull overcomes the radiation pressure and the star collapses. What happens next depends on how massive the remnant star is. If it is lighter than the Chandrasekhar limit ($\approx 1.4 M_\odot$) [8], electron degeneracy pressure will balance the gravitational pull and a white dwarf is formed. If it is heavier than the Chandrasekhar limit, degeneracy pressure between neutrons would still be

able to prevent the collapse as long as its mass is not much greater than $\approx 2M_\odot$ [9], this result is known as the Tolman–Oppenheimer–Volkoff limit.

For objects more massive than the TOV limit there is no known physical effect that can balance gravity and the star collapses. Oppenheimer and Snyder [10] concluded that, during the collapse, the gravitational potential becomes so strong that light is trapped inside a region of spacetime separated from an outside observer by an event horizon and a black hole (BH) is formed. Hence, the idea of BHs reappears two centuries later as a possible end state for massive stars.

In 1916, Karl Schwarzschild [11] derived the first spherically symmetric vacuum solution of the Einstein field equations, describing spacetime around a massive, uncharged and static object. Although, it was only a few decades later, in 1958, that David Finkelstein understood that his solution could describe a BH with an event horizon at Schwarzschild radius [12].

Most astrophysical objects have angular momentum so it was natural to assume that BHs were no exception. Solving Einstein field equations for a rotating BH was a tremendous task performed by Roy Kerr in 1963 [13], his solution is known as - the Kerr solution.

Although intriguing, BHs are thought to be relatively simple astrophysical objects, being completely described with, at most, 3 parameters: their mass M, angular momentum J and charge Q. This property results from the uniqueness theorem, which was derived independently by Israel [14], Carter [15] and Robinson [16]. It is, however, not feasible to have an isolated charged astrophysical object in the universe. If such an object existed, it would be quickly neutralised by the surrounding plasma. Thus, BH candidates are expected to be well described by the Kerr solution, which depends only on their mass and spin.

A BH candidate must be heavier than the neutron star limit $\sim 3M_\odot$ [17], not larger than its Schwarzschild radius and must not emit any electromagnetic radiation. BH candidates mass is usually inferred from orbital parameters or observations of nearby gas dynamics.

There are two main categories of BH candidates: stellar-mass BHs [18] and supermassive BHs [19]. Stellar-mass BHs have small masses $M \sim 3-100M_\odot$ and result from the collapse of massive stars at the end of their lives. It is widely believe they are abundant in our galaxy with some estimates giving 10^8 BHs. Supermassive BHs have much larger masses $M \sim 10^5-10^{10}M_\odot$ and are usually found at the center of galaxies, constituting active galactic nuclei (AGN) and quasars. Their mechanism origin is still unclear with some theories arguing they result from mass accretion and merging with other BHs. There could exist a third, still unexplored, category of BHs: intermediate-mass BHs, which, for some reason, did not grow enough to become supermassive BHs. These would have masses $M \sim 10^2 - 10^4M_\odot$, filling the gap between stellar-mass and supermassive BHs.

1.3 Black hole mimickers

Even though astrophysical BH candidates do not correspond to perfect vacuum solutions, e.g., most of the times they are surrounded by matter forming an accretion disk (AD), it is widely believed they are well described by the Kerr solution.

There are, however, two strong reasons for questioning the Kerr paradigm and looking for

other solutions that could potentially describe BHs. One is related to the existence of dark matter (DM) in the universe and the other is related to the pathological behaviour inside the event horizon.

DM is a large fraction of, presumably non-baryonic, matter in the universe which interacts weakly with light, thus being dark, which is responsible for the huge gravitational attraction required to explain velocity curves in spiral galaxies [20]. DM is thought to be overwhelmingly more abundant than baryonic matter described by the Standard Model, constituting, approximately, 27% of the universe's mass [21]. There is strong evidence supporting its existence: gravitational lensing, the cosmic microwave background, the formation and evolution of galaxies, and galaxies dynamics within galaxy clusters. DM also plays an important role in the cosmological lambda - cold dark matter model Λ_{CDM} explaining the formation of structures in the universe, without which some galaxies should not exist at all.

We are lacking, however, a theory to understand its nature. Despite the strong belief that it is non-baryonic, it could consist of faint astrophysical objects such as brown dwarfs, BHs or neutron stars, constituting massive compact halo objects [22]. Even considering that they could explain some DM mass, it is unlikely that they can account for the entire DM content of the universe. Nowadays, most DM models are based on new and undiscovered particles not included in the standard model such as axions [23, 24], originally introduced to explain the absence of CP violation in QCD, and weakly interacting massive particles (WIMPS) [25].

Therefore, in the same way baryonic matter forms structures like stars, DM particles could also form localised and stable solutions of the Einstein field equations that could be as massive and compact as BH solutions.

On the other hand, GR predicts that as we approach the singularity, matter density and spacetime curvature grow infinite, suggesting that the theory breaks down closer to this limit. Despite the current belief that this would not happen in a quantum theory of gravity, i.e., a theory of gravity compatible with quantum mechanics, such a theory does not exist. This motivates the search for alternative solutions with a regular behaviour that could describe BH candidates.

The best way to test the Kerr paradigm is to consider other astrophysical objects, known as BH mimickers, that could mimic the observations of BH candidates and compare them against experimental data.

BH mimickers are solutions of the Einstein field equations which are hard to distinguish observably from BHs but do not have an event horizon. Some possibilities discussed nowadays as possible BH mimickers are wormholes [26], gravastars [27, 28], brane world solutions [29] and boson stars (BS) [30]. There are two lines of approach for studying BH mimickers. One consists in describing BHs under new theoretical frameworks, which usually do not include rotation, and devising experiments for testing them. Another approach is to constrain possible deviations from the Kerr spacetime, which could arise from macroscopic quantum effects, the presence of exotic matter or classical extensions of GR [31].

An important property regarding these objects is stability: it has been shown that wormhole solutions supported by phantom scalar fields are unstable [32], while gravastars [33] and boson stars [34] have well-established stability regions.

Most tests regarding astrophysical objects analyse gravitational and electromagnetic

waves emitted by them or in their surroundings, which encode information on the background metric. There is an ongoing effort to identify signatures that could motivate the existence of such solutions and infer their properties, such as spin and mass.

Just like BHs, BH mimickers will show particular signatures in gravitational waves emission from a perturbation analysis or binary collisions. In fact, some have been proposed for the case of gravastars [35] and BSs[36]. However, not all objects allow for a perturbation analysis, as is the case of most wormhole models, which have a short lifetime.

Most electromagnetic radiation from BH candidates comes from the surrounding AD. Observational signatures in disks emission spectrum have been discussed for many BH mimickers as is the case of BSs [37], rotating gravastars [38], brane-world BHs [39] and wormholes [40].

BSs consist of self-gravitating time-dependent scalar fields, which have been studied as a toy model for exotic matter in the universe, such as DM halos [41] and BH mimickers [42]. Despite not existing strong evidence supporting them, the confirmation of the Higgs boson detection [43] at CERN in 2013 motivated the existence of scalar fields in the universe, which could form self-gravitating solutions.

In this work, we are interested in studying if the weak field limit of BS, known as Newtonian boson stars (NBSs), could behave as BH mimickers. NBSs are thought to be made out of very light boson fields of mass $\mu \sim 10^{-22} eV$ and have been studied in the context of fuzzy (light) DM to account for the small-scale observations incompatible with CDM models [44].

1.4 Testing strong field gravity

Einstein theory of GR, despite being elegant and mathematically robust, still needed to surpass the test of experiment. Einstein proposed three tests in 1916: explain the perihelion precession of Mercury's orbit, light deflection by the Sun and gravitational redshift of light.

The first test of GR happened right after the publication of the theory in 1916. Considering GR effects, Einstein ended a six decades conundrum, finally explaining the perihelion precession of Mercury's orbit, which mainly occurs due to perturbations from the other planets. However, the first big success of the theory happened when Eddington, a renowned astrophysicist of the time, went on an expedition to the island of Principe and measured the light deflection by the Sun during a solar eclipse.

Thus, within the first decades after the publication of GR, the theory was successfully tested, mostly with observations in the solar system where gravity is weaker. Some tests as the measurement of gravitational redshift, i.e., particles losing energy when travelling against a gravitational field, and the observation of gravitational lensing were only made possible by technological advances in 1954 and 1979, respectively.

GR becomes even more fascinating when considering the strong field regime, where gravity is extreme. The theory predicts, among other things, the existence of BHs with spacetime singularities of infinite density and spacetime curvature enclosed by an event horizon. Understanding if such objects exist in the universe and how accurately described by GR theory they are is one of the major challenges we face in astrophysics.

Since it is impossible to observe a BH directly, its existence and properties have to be sustained from indirect observations.

Most stellar BH candidates are believed to be in binary systems, either with another BH, a neutron star or a regular star. When the star companion loses matter, mainly through the Roche lobe of the binary potential, a flattened band of spinning matter is formed around the BH, an AD. Friction between adjacent rotating layers in the disk makes matter slowly lose angular momentum and spiral toward the BH. The disk gets hotter close to its inner edge, making stellar mass BH the brightest source of X-rays in the sky. The first BH candidate considered was the bright X-ray source Cygnus X-1 in 1973 [45], with a mass $M \approx 21 M_{\odot}$.

The AD spectrum depends on the properties of the disk and the surrounding spacetime. Besides affecting the structure of the disk itself, e.g., the location of its inner edge depends on the BH spin, spacetime curvature bends the trajectory of photons emitted from the disk making them lose energy. Thus, the AD spectrum is a powerful tool to probe spacetime, study the central compact object and ultimately test general relativity. In fact, most measurements of BH spin come from X-ray spectroscopy related to the AD spectrum [46].

So far most observations of BH candidates relied on electromagnetic radiation. The paradigm changed when in 2016, LIGO and VIRGO [47] collaborations confirmed the detection, for the first time, of gravitational waves from a binary BH merger. Gravitational waves are a theoretical prediction of GR, consisting of spacetime ripples resulting from the motion of massive bodies. They constitute ideal probes of spacetime as they interact very weakly with matter and show little dispersion, carrying along information of the source metric. BH binaries are expected to be strong sources of gravitational waves, especially during in-spiral, merger and ring-down phases. This makes them ideal for testing GR in the strong field regime and understanding the nature of BH candidates.

In 2019, another breakthrough happened when the Event Horizon Telescope presented the first image of the shadow of the BH at the centre of galaxy M87 [48]. The shadow of a BH consists of a large dark area in the centre against a bright background and is formed by the gravitational lensing of the BH event horizon. In 2022, the collaboration released the first image of the supermassive BH at the centre of our galaxy - Sgr A* [49].

So far, all observations of BH candidates are consistent with the Kerr paradigm. Despite existing many approaches for studying the nature of these compact objects, mainly through the study of electromagnetic and gravitational waves, we will focus on electromagnetic observations related to ADs.

1.5 Accretion disks

To understand the AD spectrum and relate it with BH properties like the spin, we first need a theoretical framework for the disk's structure.

Broadly speaking, an AD consists of a band of spinning matter around a central accreting object. AD study is a vibrant research field as there is a widespread view that they are linked to a variety of astrophysical phenomena such as star and planetary formation and associated with the most energetic events in the universe as is the case of X-ray binaries and AGNs.

In 1969, Lynden-Bell [50] argued that viscosity stresses in ADs could be powering AGNs by converting the gravitational energy of the accreted matter into radiation. Despite the strong motivation for AD theory, we were still lacking a mathematical description modelling the dynamics of the accretion flow.

Finally, in 1973 Shakura and Sunyaev [51] proposed the standard model of ADs, also known as the α-disk model. The model presents a Newtonian analytical solution for an equatorial, geometrically thin and optically thick disk around a static BH. However, some well-known results from GR were incorporated into the model, e.g., the inner edge of the disk was assumed to be at innermost stable orbit radius. The model is commonly referred to as α-disk because an α parameter was introduced to account for the turbulent viscosity in the disk.

Remarkably soon after the publication of the α-disk model, in 1974, a relativistic version of the theory was elaborated by Novikov and Thorne [52, 53] describing the accretion process for a Kerr BH. In the following decades, several AD models with different geometries and including new effects have been proposed: the polish doughnut disk, the slim disk and the advection-dominated accretion flows are a few examples.

Disk viscosity is a crucial part of the model as it is responsible for the angular momentum transport mechanism and for generating friction, making the disk radiate. In 1991, Balbus and Hawley [54] discussed that weak magnetic fields present in the disk could originate instabilities, known as magnetorotational instabilities, responsible for the emergence of turbulent viscosity.

Nowadays, the AD paradigm is a fully established theory, largely sustained by experiments and it has proven to be a powerful tool to study BH candidates, especially using X-ray spectroscopy.

X-ray spectroscopy is a technique for measuring the spin of BH candidates and is based on two methods: the continuum fitting [55], which analyses the thermal spectrum of the AD, and the reflection spectroscopy, which analyses the most prominent feature of the reflection spectrum, the Fe K_α line [56]. While the latter may be used to study all kinds of BHs, the continuum fitting technique can be applied to supermassive BHs as they emit in optical/UV bands for which measurements are noisier due to dust absorption [46].

1.6 Outline

The focus of this project is to understand if compact objects made of light boson fields could mimic BH accretion.

In chapter 2, we introduce the Kerr spacetime and review some circular orbit properties, which are fundamental for describing the accretion process. Starting from the Poisson-Schrödinger equation, we derive the elementary properties of the Newtonian boson stars in chapter 3. In chapter 4, we discuss the accretion flow dynamics and how they influence BH evolution, presenting the Novikov-Thorne model and introducing Thorne's limit. Additionally, we describe how X-Ray Spectroscopy is used to survey gravity in the strong field regime. In chapter 5, we compare the properties of AD around NBSs with the ones around BHs,

discussing The project conclusions and final remarks are presented in chapter 6.

Chapter 2

Black holes

In this chapter geometrized units $c = G = 1$ will be used. The Kerr line element for a BH of mass M and spin J, rotating in the ϕ direction, in Boyer–Lindquist coordinates (t,r,θ,ϕ) can be written as

$$ds^2 = -\left(1 - \frac{2Mr}{\Sigma}\right) dt^2 - \frac{4aMr\sin^2\theta}{\Sigma} dt d\phi + \frac{\Sigma}{\Delta} dr^2 + \Sigma d\theta^2 + \left(r^2 + a^2 + \frac{2a^2 Mr\sin^2\theta}{\Sigma}\right) d\phi^2, \quad (2.1)$$

where $\Sigma = r^2 + a^2\cos^2\theta$, $\Delta = r^2 - 2Mr + a^2$ and $a = J/M$. The metric describes stationary and axisymmetric spacetime about the polar axis and, when considering a static BH $a = 0$, we recover the Schwarzschild solution.

The metric is singular for $\Sigma = 0$ and $\Delta = 0$ but only the first represents a physical singularity where spacetime curvature is infinite, for $r = 0$ and $\theta = \pi/2$. The second condition give us the event horizon radius for the Kerr spacetime

$$r_{EH} = M + \sqrt{M^2 - a^2}. \quad (2.2)$$

The square root in (2.2) implies that for a BH to exist it requires $|a| < M$, otherwise it would have a naked singularity, i.e., a singularity not hidden by an event horizon, violating the cosmic censorship conjecture [57]. Let us also define, for the sake of simplicity, a spinning parameter $a^* = J/M^2 = a/M$ that varies from $a^* = 0$ for a Schwarzschild BH to $a^* = 1$ for a maximal spinning Kerr BH.

2.1 Circular orbits in axisymmetric spacetimes

We are interested in studying AD dynamics where we assume particles undergo nearly circular geodesic motion. The spectrum of the disk depends on quantities related to particle orbital motion: its specific energy E, specific angular momentum L and orbital velocity Ω_ϕ.

We will analyse a test particle circular orbital motion along the equatorial plane, deriving

expressions for E, L and Ω_ϕ. A generic time-independent axisymmetric spacetime will be considered since these results are also useful for describing the accretion flow around NBS.

We start by considering a line element of the form

$$ds^2 = g_{tt}dt^2 + g_{rr}dr^2 + g_{\phi\phi}d\phi^2 + 2g_{t\phi}dtd\phi + g_{\theta\theta}d\theta^2, \tag{2.3}$$

note that we neglect the term g_{rt} as we can always find a coordinate transformation such that it vanishes.

The particle's equations of motion can be obtained by applying the variational principle to the geodesics lagrangian

$$\mathcal{L}_G = \frac{1}{2}g_{\alpha\beta}\dot{x}^\alpha\dot{x}^\beta. \tag{2.4}$$

Defining λ as any parameter along the world line, e.g., the particle's proper time for time-like geodesics, we can write the Euler-Lagrange equation as

$$\frac{d}{d\lambda}\left(\frac{\partial\mathcal{L}_G}{\partial\dot{x}^\alpha}\right) - \frac{\partial\mathcal{L}_G}{\partial x^\alpha} = 0, \tag{2.5}$$

where $\dot{x}^\alpha = \frac{dx^\alpha}{d\lambda}$. Considering only motion along the equatorial plane $\theta = \frac{\pi}{2}$ and $d\theta = 0$. As spacetime is time independent and axisymmetric this implies that the lagrangian does not depend explicitly on t nor ϕ. According to Noether's theorem these two symmetries originate two conserved quantities: energy $E = -P_t = \frac{\partial\mathcal{L}_G}{\partial\dot{t}}$ and angular momentum $L = P_\phi = \frac{\partial\mathcal{L}_G}{\partial\dot{\phi}}$.

Using the definition of E and L, we can express them as function of the metric components and velocities $\dot{t}$ and $\dot{\phi}$

$$E = -g_{tt}\dot{t} - g_{t\phi}\dot{\phi}, \tag{2.6}$$

$$L = g_{\phi\phi}\dot{\phi} + g_{t\phi}\dot{t}. \tag{2.7}$$

Rearranging the previous equations we find $\dot{t}$ and $\dot{\phi}$

$$\dot{t} = \frac{g_{\phi\phi}E + g_{t\phi}L}{g_{t\phi}^2 - g_{tt}g_{\phi\phi}}, \quad \dot{\phi} = -\frac{g_{t\phi}E + g_{tt}L}{g_{t\phi}^2 - g_{tt}g_{\phi\phi}}. \tag{2.8}$$

Using the expressions (2.8) and the conservation of rest mass $g_{\mu\nu}\dot{x}^\mu\dot{x}^\nu = -1$ we obtain

$$g_{rr}\dot{r}^2 + g_{\theta\theta}\dot{\theta}^2 = V_{\text{eff}}(E, L, r, \theta), \tag{2.9}$$

where

$$V_{\text{eff}}(E, L, r, \theta) = \frac{g_{\phi\phi}E^2 + 2g_{t\phi}EL + g_{tt}L^2}{g_{t\phi}^2 - g_{tt}g_{\phi\phi}} - 1 \tag{2.10}$$

is the effective potential of the test particle. As we are restricting ourselves to circular orbits along the equatorial plane we must require $\dot{r} = \dot{\theta} = 0$ and $\ddot{r} = \ddot{\theta} = 0$, the first condition implies $V_{\text{eff}} = 0$ the second implies $\partial_r V_{\text{eff}} = 0$. Solving the system of equation give us explicit expressions for Ω_ϕ (2.11), E (2.12) and L (2.13).

$$\Omega_\phi = \frac{\dot{\phi}}{\dot{t}} = \frac{-\partial_r g_{t\phi} \pm \sqrt{\left(\partial_r g_{t\phi}\right)^2 - \partial_r g_{tt}\partial_r g_{\phi\phi}}}{\partial_r g_{\phi\phi}} \tag{2.11}$$

$$E = -\frac{g_{tt} + g_{t\phi}\Omega_\phi}{\sqrt{-g_{tt} - 2g_{t\phi}\Omega_\phi - g_{\phi\phi}\Omega_\phi^2}} \tag{2.12}$$

$$L = \frac{g_{t\phi} + g_{\phi\phi}\Omega_\phi}{\sqrt{-g_{tt} - 2g_{t\phi}\Omega_\phi - g_{\phi\phi}\Omega_\phi^2}} \tag{2.13}$$

We also present the expressions of Ω_{BH} (2.14), E_{BH} (2.15) and L_{BH} (2.16) for the case of orbital motion around a Kerr BH, where the upper (lower) sign represents a particle whose momentum is parallel (anti-parallel) to the BH spin.

$$\Omega_{BH} = \pm\frac{M^{1/2}}{r^{3/2} \pm aM^{1/2}} \tag{2.14}$$

$$E_{BH} = \frac{r^{3/2} - 2Mr^{1/2} \pm aM^{1/2}}{r^{3/4}\sqrt{r^{3/2} - 3Mr^{1/2} \pm 2aM^{1/2}}} \tag{2.15}$$

$$L_{BH} = \pm\frac{M^{1/2}\left(r^2 \mp 2aM^{1/2}r^{1/2} + a^2\right)}{r^{3/4}\sqrt{r^{3/2} - 3Mr^{1/2} \pm 2aM^{1/2}}} \tag{2.16}$$

2.2 Innermost stable circular orbits - ISCO

Unlike what happens in Newtonian mechanics, not all circular orbits for test particles orbiting BHs are stable in GR. There is a boundary beyond which all inner circular orbits are unstable and particles plunge directly into the BH. This boundary is known as the innermost stable orbit (ISCO). In Newtonian mechanics, circular orbital motion requires balancing the gravitational pull with the centrifugal force. However, near the BH horizon, the gravitational pull gets so intense that the centrifugal force can not balance it. Thus, stable circular orbital motion does not exist close to BHs. As most AD models assume the inner edge of the disk is at ISCO radius, it is essential to understand how r_{ISCO} varies with BH mass and spin.

All circular orbits which verify $\partial_r^2 V_{\text{eff}} \geq 0$ are stable. In order to find r_{ISCO}, we must solve the limiting condition for stability $\partial_r^2 V_{\text{eff}} = 0$. In 1972, Bardeen [58] derived an expression for r_{ISCO} in Boyer–Lindquist coordinates as a function of the BH spin a^*:

$$r_{ISCO} = M\left\{3 + Z_2 \mp \left[(3 - Z_1)\left(3 + Z_1 + 2Z_2\right)\right]^{1/2}\right)\right\}, \tag{2.17}$$

where

$$Z_1 = 1 + \left(1 - \frac{a^2}{M^2}\right)^{1/3}\left[\left(1 + \frac{a}{M}\right)^{1/3} + \left(1 - \frac{a}{M}\right)^{1/3}\right],$$

$$Z_2 = \left(3\frac{a^2}{M^2} + Z_1^2\right)^{1/2},$$

where the upper (lower) sign represents a corotating (counter-rotating) orbiting particle.

Figure 2.1 represents how the r_{ISCO} (2.17) and r_{EH} (2.2) vary with BH spin a^*.

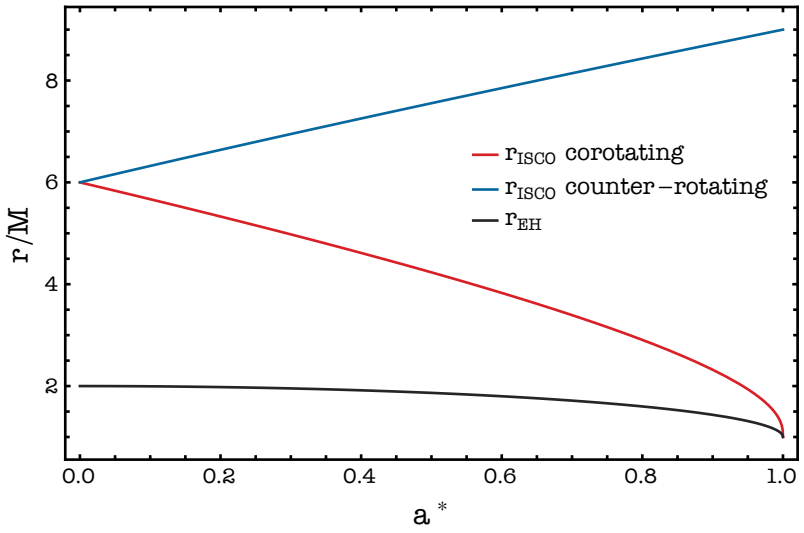

Figure 2.1: r_{ISCO} and r_{EH} as function of the BH spin a^*

We observe that $r_{ISCO} = 6M$ for an orbiting particle around a Schwarzchild BH. When considering a Kerr BH, we find that r_{ISCO} for corotating orbiting particles is always smaller than the one of counter-rotating orbiting particles.Thus, corotating particles can develop stable orbits much closer to the BH. For a maximal Kerr spinning BH, $r_{ISCO} = 9M$ for the case of counter-rotating particles, and $r_{ISCO} = M$ for corotating ones.

Chapter 3

Newtonian boson stars

In this section we will use $\hbar = c = G = 1$. BSs are localised and stable solutions of a complex scalar field Φ coupled to gravity. Unlike ordinary stars where the nuclear reactions in the core generate pressure which balances their gravitational pull, in BSs the balancing pressure arises from the Heisenberg principle. In 1964, Derrick [59] proved that no time stable localzied solutions with finite energy exist. However, the stress-energy tensor $T^S_{\mu\nu}$ (3.7) only depends on the absolute value of the scalar field $|\Phi|^2$. We would still obtain a time-independent gravitational field by considering a time-periodic scalar field

$$\Phi = \Psi(r)e^{-i\Omega t}, \tag{3.1}$$

where $\Psi(r)$ is a real function which statisfies the boundary conditions $\partial_r\Psi(0) = 0$ and $\lim_{r\to\infty}\Psi(r) = 0$ and Ω is the energy of the field.

3.1 NBS spacetime

In order to describe the accretion process of a NBS and compare it with the one of a BH, we need to find the metric for a NBS.

We start from the action $\mathcal{S}$ of a massive complex scalar field Φ minimally coupled with gravity

$$\mathcal{S} \equiv \int \sqrt{-g}\left(\frac{R}{16\pi} - \frac{1}{2}g^{\mu\nu}\partial_\mu\Phi\partial_\nu\Phi^* - \mathcal{U}(|\Phi|^2)\right)d^4x, \tag{3.2}$$

where R is the Ricci scalar of the metric, $g = det(g_{\mu\nu})$ is the metric determinant and Φ^* is the field complex conjugate. The first term of $\mathcal{S}$ is the Einstein-Hilbert action, the second term is the kinetic term and the last term is a self-interaction potential $\mathcal{U}$.

Admitting a weak scalar field $|\Phi| \ll 1$, we will consider a simple mass term potential and neglect higher order terms

$$\mathcal{U} \sim \frac{\mu^2}{2}|\Phi|^2 + \mathcal{O}\left(|\Phi|^4\right), \tag{3.3}$$

where μ is the scalar field mass.

The action $\mathcal{S}$ (3.2) enjoys a $U(1)$ symmetry, i.e., is invariant under a global phase rotation $\Phi \to \Phi e^{i\alpha}$, which, according to Noether's theorem, implies the existence of the conserved current

$$j^{\mu} = -\frac{ig^{\mu\nu}}{2}(\Phi^* \partial_\nu \Phi - \Phi \partial_\nu \Phi^*) \tag{3.4}$$

and the associated conserved charged

$$Q = \int_{\Sigma} d^3x \sqrt{-g} j^t, \tag{3.5}$$

where the integration is performed over a spacelike hypersurface of constant time Σ and j^t is the time component of the 4-current. The conserved Noether charge Q corresponds to the total number of bosons in the BS. If we have considered a local $U(1)$ symmetry for the action, that would lead to charged NBS [60].

Varying the action with respect to Φ^* and $g_{\mu\nu}$, we obtain a coupled system of field equations for complex field Φ and the metric field $g_{\mu\nu}$, the Einstein-Klein-Gordon system:

$$\begin{aligned} &\frac{1}{\sqrt{-g}} \partial_\mu \left(\sqrt{-g} g^{\mu\nu} \partial_\nu \Phi \right) = \mu^2 \Phi \\ &R_{\mu\nu} - \frac{1}{2} R g_{\mu\nu} = 8\pi T^S_{\mu\nu}, \end{aligned} \tag{3.6}$$

where $R_{\mu\nu}$ is the Ricci tensor and $T^S_{\mu\nu}$ (3.7) is the stress-energy tensor of the scalar field.

$$T^S_{\mu\nu} = \partial_\mu \Phi^* \partial_\nu \Phi - \frac{1}{2} g_{\mu\nu} \left[\partial_\alpha \Phi^* \partial^\alpha \Phi + 2U\left(|\Phi|^2\right) \right] \tag{3.7}$$

A NBS is made out of individual scalar particles with an energy, approximately, given by their rest-mass energy $\Omega \approx \mu$. The spacetime metric in the weak field limit [61] can be written as

$$ds^2 = -(1 + 2\mathcal{U}) dt^2 + dr^2 + r^2 \left(d\theta^2 + \sin^2\theta d\varphi^2 \right). \tag{3.8}$$

Assuming Φ is non-relativistic, the system of field equations can be simplified to leading order terms, obtaining the Schrödinger-Poisson system (3.9), where $\widetilde{\Phi}$ is the Schrödinger field, which relates to the Dirac field Φ by the transformation $\widetilde{\Phi} = \sqrt{\mu} e^{i\mu t} \Phi$.

$$\begin{aligned} &i\partial_t \widetilde{\Phi} = -\frac{1}{2\mu} \nabla^2 \widetilde{\Phi} + \mu \mathcal{U} \widetilde{\Phi} \\ &\nabla^2 \mathcal{U} = 4\pi\mu |\widetilde{\Phi}|^2 \end{aligned} \tag{3.9}$$

Using the ansatz (3.1) we obtain a simplified system of field equations that can be solved numerically :

$$\begin{aligned} &\partial_r^2 \Psi + \frac{2}{r} \partial_r \Psi - 2\mu(\mu\mathcal{U} + \gamma)\Psi = 0, \\ &\partial_r^2 \mathcal{U} + \frac{2}{r} \partial_r U - 4\pi\mu^2 \Psi^2 = 0, \end{aligned} \tag{3.10}$$

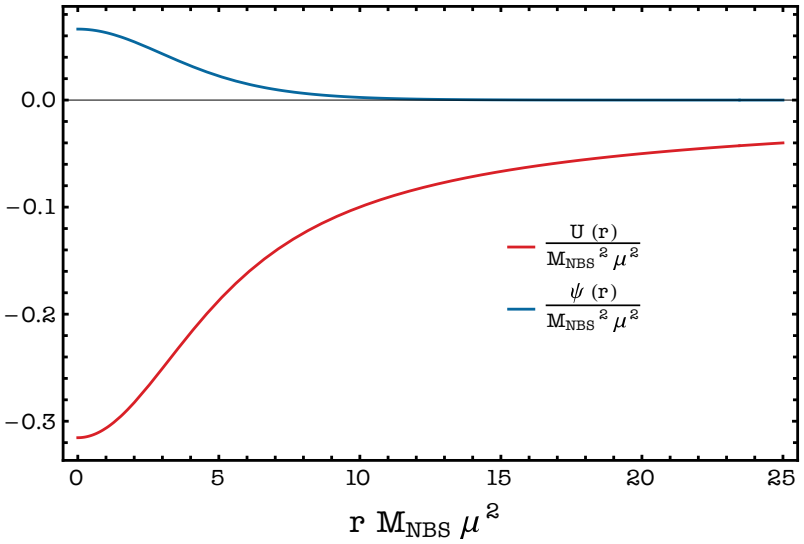

Figure 3.1: Potential radial profiles of the potential $\mathcal{U}(r)$ and the scalar field $\Psi(r)$, describing all the fundamental NBS.

with the constraints $|\Psi| \ll 1$, $|\mathcal{U}| \ll 1$ and $\Omega \approx \mu$.

One can observe that the system (3.10) is left invariant under the scaling transformation

$$(\Psi, \mathcal{U}, \gamma) \to \lambda^2(\Psi, \mathcal{U}, \gamma) \quad r \to r/\lambda, \tag{3.11}$$

where λ is a scaling parameter. Defining the mass of a NBS M_{NBS} as

$$M_{\text{NBS}} = 4\pi\mu^2 \int_0^\infty r^2 |\Psi|^2 dr \tag{3.12}$$

these scaling transformations simply mean that we are scaling M_{NBS} as $M_{\text{NBS}} \to \lambda M_{\text{NBS}}$.

This result is extremely useful since once a fundamental solution is found, by solving the system of field equations (3.10), we can always find a parameter λ to rescale the solution and obtain new NBSs solutions of different masses M_{NBS} without having to solve the system explicitly again. Given a sufficiently small λ parameter, the rescaled solution will also satisfy the constraints on μ, $\mathcal{U}$ and Ψ.

A numerical solution of the system of field equations describing all fundamental NBSs' potential is described in figure 3.1. The NBS gravitational potential $\mathcal{U}$, unlike the BH one, is regular close to the origin. This result will be extremely important for explaining the differences in the ADs dynamics between BHs and NBSs.

We observe that $\mathcal{U}$ asymptotically behaves as a Newtonian potential $\mathcal{U} \sim -M_{NBS}/r$, while Ψ decays exponentially for larger radii.

The definition of a NBS's radius R is ambiguous since NBSs have no surface and the field Ψ extends to infinity. A reasonable definition, commonly used in the literature, is to define R as the radius of a sphere containing 98% of the mass.

All fundamental NBSs satisfy the mass-radius relation

$$M_{NBS}\mu = \frac{9.1}{R\mu}, \tag{3.13}$$

which implies that as a NBS shrinks it gets more massive.

We numerically found an expression for M_{NBS} as a function of the scaling parameter λ, the field's mass μ and the radius R

$$\frac{M}{M_\odot} \approx 2.4 \times 10^6 \, \lambda \left(\frac{10^{12} m}{R}\right) \left(\frac{10^{-17} eV}{\mu}\right)^2. \tag{3.14}$$

It exists, however, a limit to a NBS radius: the Schwarzschild radius $R = 2M_{NBS}$, below which spacetime is described by a BH solution. Intuitively, this suggests the existence of a maximal mass for BSs. This limit was computed for the case of non-interacting scalar fields and the result is known as Kaup mass limit M_{Kaup}, assuming the value $M_{Kaup}\mu \approx 0.63$.

Since the validity of the Newtonian regime implies that all NBS solutions considered must verify the conditions $|\Psi| \ll 1$, $|\mathcal{U}| \ll 1$ and $\Omega \approx \mu$, we impose a mass limit of $M_{NBS}\mu \leq 0.55$ which corresponds to a potential $\mathcal{U} \approx -0.095$ and to a field $\Psi \approx 0.02$.

3.2 Circular orbits

Unlike what happens for BHs, all circular orbits around a NBS are stable,i.e., $r_{ISCO} = 0$. As the NBS metric is axisymmetric and time independent, depending only on M_{NBS} and μ, we can use the results of the previous chapter to compute E (2.12), L (2.13) and Ω_ϕ (2.11) for circular orbits around NBSs.

Figure 3.2 represents the radial profiles of E, L and Ω for a test particle undergoing circular equatorial orbital motion around a NBS and a BH with the same mass.

An incoming particle from infinity releases gravitational energy E and loses angular momentum L as it increases its orbital velocity Ω_ϕ. The E_{BH} and L_{BH} profiles have a minimum for r_{ISCO}, below which they increase drastically. However, this does not occur for a NBS where E_{NBS} and L_{NBS} decrease steadily until $r = 0$. A similar behaviour can be observed for the angular velocity, Ω_{NBS} increases steadily until $r = 0$ and Ω_{BH} increases infinitely, closer to the origin.

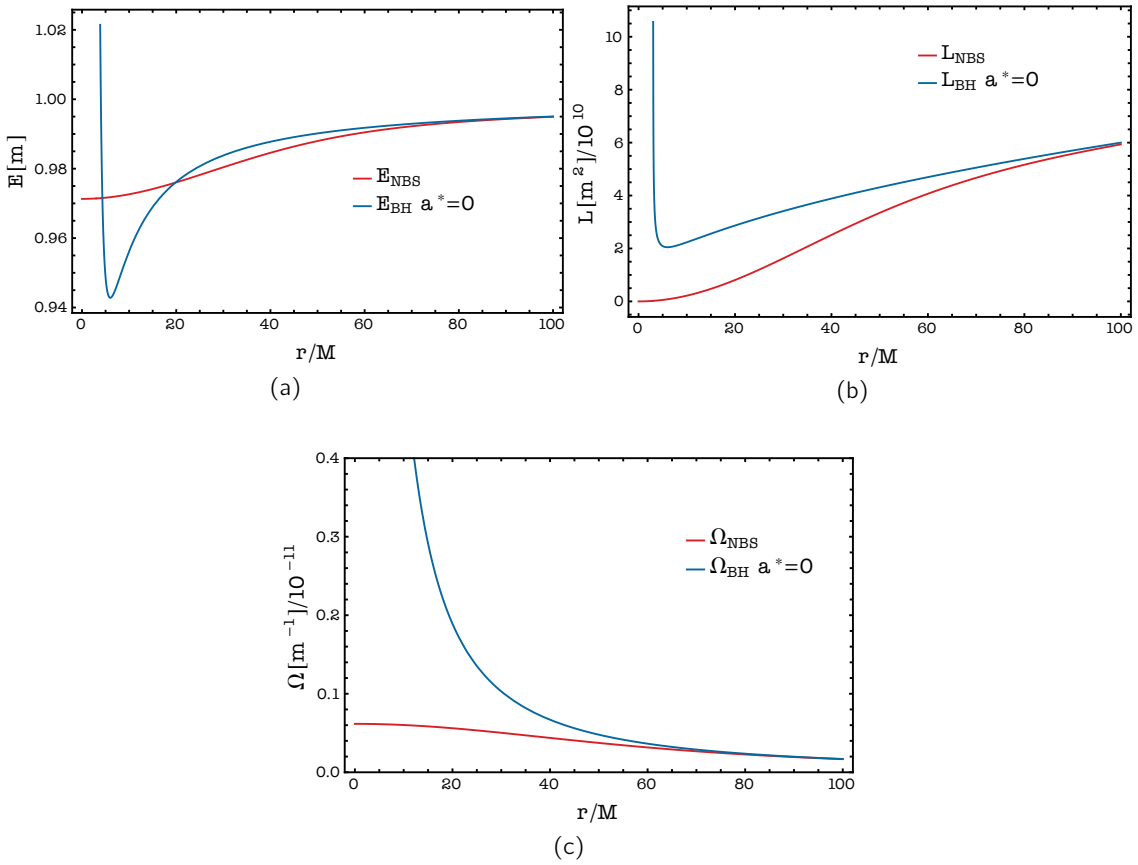

Figure 3.2: Radial profiles of the specific energy E (a), specific angular momentum L (b) and angular velocity Ω (c) for a test particle undergoing circular equatorial orbital motion around a NBS, with a field mass $\mu = 10^{-17} eV$, and a BH with the same mass $M = 4 \times 10^6 M_\odot$.

Chapter 4

Accretion disks

The accretion flow dynamics is described by a set of non-linear, coupled differential equations of magnetohydrodynamics which is complex to be solved analytically.

Usually one makes a few assumptions about the geometry and optical thickness of the disk that allow us to simplify the model. If the horizontal extension of the disk r is much larger than the vertical extension of the disk (height H) the disk is considered to be thin ($H/r \ll 1$). If the photons mean free path is smaller than the height of the disk, the disk is considered to be optically thick and most of the thermal emission will happen at the surface of the disk.

In this work, we will describe the accretion process around a steady, equatorial, geometrically thin and optically thick accretion disk. The disk geometry is well described with cylindrical coordinates (t, r, Φ, z) with an half-thickness $h(r)$ such that its vertical extension varies from $-h$ to h, vanishing for the inner edge of the disk at r_{in}.

Matter flowing toward the central compact object has considerable angular momentum, thus rotating around it in nearly circular geodesics. When matter loses angular momentum and moves to an inner (faster) orbit, an outer (slower) orbit gains momentum, originating a continuous flow of momentum to the outermost part of the disk. There must exist an angular momentum transport mechanism responsible for carrying it away as matter approaches the centre. This angular momentum transport mechanism is originated from magnetic fields, turbulence and viscosity present in the disk. Then, matter's differential rotation originates tangential stresses responsible for heating the disk and making it radiate.

The AD flux is highly determined by its accretion rate . One can usually obtain a reasonable estimate for $\dot{M}$ from Eddington accretion rate $\dot{M}_{Edd}$. The $\dot{M}_{Edd}$ corresponds to the accretion for which matter's gravitational pull perfectly balances its radiation pressure. For $\dot{M} > \dot{M}_{Edd}$ extensive mass losses through stellar winds start to occur from the outermost portion of the disk.

We can estimate $\dot{M}_{Edd}$ as a function of the central compact object mass M

$$\dot{M}_{Edd} = \frac{L_{Edd}}{\eta c^2}, \tag{4.1}$$

where L_{Edd} is the Eddington luminosity and η is the accretion efficiency. η depends on

the nature of the accretion process and the background metric and describes how efficient the accretion process is at converting rest mass into heat, which is then radiated away as luminosity. For a static BH, $\eta \approx 5.7\%$ and for a maximally rotating one, $\eta \approx 42\%$ while estimates from AGNs require $\eta \approx 0.1$. Taking $\eta = 0.1$ we can define $\dot{M_{Edd}}$ as

$$\dot{M}_{Edd} = 2.218 \times 10^{-2} \left(\frac{M}{10^6 M_\odot} \right) M_\odot / year \tag{4.2}$$

However, astrophysical accretion rate flows must be smaller than $\dot{M}_{Edd}$. One usually estimates $\dot{M}$ from the Eddington ratio f_{Edd} such that

$$\dot{M} = f_{Edd}\, \dot{M}_{Edd}, \tag{4.3}$$

where $f_{Edd} \sim 10^{-4}$ for most AGNs[62].

4.1 Shakura and Sunyaev model

The α-disk model presents a classical description of the accretion flow dynamics for a steady geometrically thin and optically thick disk around a static accreting BH. The model assumes that the inner edge of the disk r_{in} is at the ISCO radius r_{ISCO}. Besides, in the α-disk model, the disk's particle motion is mostly determined by the gravitational field of the accreting object, neglecting the presence of magnetic fields and the influence of gas pressure.

Assuming matter rotation in the disk is Keplerian, we can write the orbital velocity Ω as

$$\Omega_\phi = \sqrt{\frac{GM}{r^3}}. \tag{4.4}$$

For the sake of convenience let us define a surface density of matter Σ by integrating the disk's mass density ρ along the vertical direction

$$\Sigma = \int_{-h}^{h} \rho dz, \tag{4.5}$$

where h is the half-thickness of the disk.

Let us also define the vertically integrate stress $W_{r\phi}$ between adjacent rotating rings on the disk

$$W_{r\phi} = \int_{-h}^{h} w_{r\phi} dz = -\alpha \Sigma c_s, \tag{4.6}$$

where α is a parameter describing the efficiency of the angular momentum transport mechanism and c_s is the speed of sound.

The structure and the energy flux of an AD in the $\alpha-$model can be derived from the conservation equations of energy, mass and angular momentum along the radial and vertical direction. The model also considers a transport equation to describe how radiation reaches the surface of the disk and an equation of state for the disk's plasma.

The flow of matter in the disk is described by the continuity equation, establishing the conservation of mass. In a steady-state regime, the continuity equation can be written as

$$\nabla \cdot (\rho \vec{u}) = 0, \tag{4.7}$$

where $\vec{u}$ is the particle's velocity.

Using Gauss's law and integrating the continuity equation in cylindrical coordinates we obtain the AD's accretion rate $\dot{M}$:

$$\dot{M} = 2\pi r u_r \Sigma, \tag{4.8}$$

where u_r is the inward radial velocity of matter.

The conservation of angular momentum along the radial direction is described by the Navier-Stokes equation. Integrating the equation along the z-direction and expressing it in cylindrical coordinates gives

$$\frac{\partial u_\theta}{\partial t} + u_r \frac{\partial}{\partial r}\left(\Omega_\phi r^2\right) = \frac{1}{r^2 \Sigma}\frac{\partial}{\partial r}(r W_{r\phi}). \tag{4.9}$$

Assuming a steady state regime, we integrate the equation (4.9) along the radial direction obtaining

$$\dot{M}\Omega_\phi r^2 = -2\pi W_{r\phi} r^2 + C, \tag{4.10}$$

where C is an integration constant. C can be determined using the fact that in the last stable orbit $r = r_{in}$ tangential stresses are expected to vanish $W_{r\phi} = 0$. Finally, we obtain an expression for the disk's stress

$$W_{r\phi} = \frac{\dot{M}\Omega_\phi}{2\pi}\left(1 - \sqrt{\frac{r_{in}}{r}}\right). \tag{4.11}$$

Neglecting the motion of the disk plasma along the vertical direction, the conservation of angular momentum simply reduces to the hydrostatic equilibrium equation

$$\frac{1}{\rho}\frac{dP}{dz} = -\frac{GM}{r^3} z, \tag{4.12}$$

where P is the pressure.

The surface pressure of the disk is much smaller than the pressure on the equatorial plane, $P(h) \ll P(z = 0)$. This allows us to find the half thickness of the disk h as a function of central pressure $P = P(z = 0)$

$$h \approx \left(\frac{P}{\rho}\right)^{1/2} \left(\frac{r^3}{GM}\right)^{1/2}, \tag{4.13}$$

where M is the mass of the central compact object.

As particles spiral towards the central compact object, they lose angular momentum and gravitational energy, increasing their rotational velocity. The energy conservation equation states that the disk flux $\mathcal{F}$ balances the work of the forces shearing stress, $-2\pi r^2 W_{r\phi}\Omega$ with the rest mass energy flow. Thus $\mathcal{F}$ can be obtained by solving the equation

$$\mathcal{F} = \frac{1}{4\pi r}\frac{d\mathcal{L}}{dr} = \frac{1}{4\pi r}\frac{d}{dr}\left[\dot{M}\left(v_\phi^2 - \frac{GM}{r}\right) - 2\pi r^2 W_{r\phi}\Omega\right]. \tag{4.14}$$

Replacing (4.11) into (4.14) yields

$$\mathcal{F} = \frac{3}{8\pi}\dot{M}\frac{GM}{r^3}\left(1 - \sqrt{\frac{r_{in}}{r}}\right). \tag{4.15}$$

The energy from stress inside the disk needs to be transported to the surface where it can be radiated away. This mechanism is described by a radiative diffusion equation

$$\varepsilon = \frac{3}{4}\frac{\sigma\mathcal{F}u_0}{c}, \tag{4.16}$$

relating, for a given flux $\mathcal{F}$, the energy density of radiation inside a layer with the surface density Σ and the disk opacity σ. Assuming the disk locally behaves as a black-body, we can estimate ϵ from the Stefan–Boltzmann law

$$\epsilon = \sigma_{SB}T^4, \tag{4.17}$$

where T is the local temperature of the disk and σ_{SB} is the Stefan–Boltzmann constant.

The black-body spectral distribution allows us to compute $L(\nu)$, the luminosity of the disk as a function of the frequency ν

$$L(\nu) = \frac{16\nu^3\pi^2 h\cos i}{c^2}\int_{r_{in}}^{R_{out}}\frac{r\,dr}{e^{h\nu/kT} - 1} \tag{4.18}$$

where i is the disk inclination, k_B is the Boltzmann constant, h is the Planck constant and r_i (r_{out}) is the inner (outer) edge of the disk.

Opacity describes how radiation is absorbed and scattered while inside the disk. There are two main contributions to the disk opacity: Thomson scattering and free-free absorption. Thomson scattering describes the scattering of radiation on free electric charges and has a cross-section of $\sigma_T \approx 6.65 \times 10^{-25} cm^2$. The free-free absorption describes the photon's scattering on free ions of the disk and has a cross-section described by Kramer's law $\sigma_{ff} \sim \rho T^{-7/2}$. Free-free absorption is the main source of opacity for the inner and hotter regions of the disk while Thomson scattering is predominant in the outer regions of the disk.

Finally, the equation of state describing matter in the disk sums the contributions of gas P_{gas} and radiation P_{rad} pressures:

$$P = P_{gas} + P_{rad} \tag{4.19}$$

Assuming the disk plasma consists mostly of ionized gas we can express P_{gas} as

$$P = \frac{2\rho K_B T}{m_p}, \tag{4.20}$$

where K_B is the Boltzmann constant and m_p is the proton's mass.

In general, P_{rad} is well approximated with

$$P_{rad} = \frac{1}{3}\epsilon. \tag{4.21}$$

We have now a system of equations that is hard to be solved analytically. In their original paper, Shakura and Sunyaev decomposed the disk into three regions and solved the system for each region, obtaining analytical estimates for the equations. They considered 3 regions: an inner region where radiation pressure dominates $c_s^2 = \epsilon/3\rho$ and disk opacity is dominated by Thomson scattering; an intermediate region where gas pressure dominates $c_s^2 = \frac{2K_BT}{m_p}$ and disk's opacity is dominated by free electron scattering and outer region where gas pressure dominates and the opacity is mostly determined by free-free absorption.

4.2 Novikov and Thorne model

In this section, we will briefly review the Novikov-Thorne model. All physical quantities will be averaged over a timescale Δt and over the azimuthal angle $\Delta\phi = 2\pi$. This allows us to neglect fluctuations in the background metric as well as inhomogeneities in the accretion flow.

The model assumes the disk particles move on the equatorial plane in nearly-circular geodesic orbits around a rotating BH of mass M. This assumption is reasonable as the pressure of the plasma is negligible in comparison with the gravitational potential of the accreting object. Thus, each particle in the disk moves in a keplerian fashion with an angular velocity Ω_ϕ, a specific energy E and a specific angular momentum L. The model assumes an angular momentum transport mechanism, as in the α-disk model, from viscous magnetic and turbulent stresses. Besides, the equatorial plane is assumed to be perpendicular to the BH's spin

The disk average surface density Σ can be obtained by integrating vertically the average rest mass density $\langle\rho_0\rangle$

$$\Sigma(r) = \int_{-h}^{h} \langle\rho_0\rangle \, dz, \tag{4.22}$$

where h is the half-thickness of the disk.

Matter in the disk can be described as an anisotropic fluid with a stress-energy tensor $T^{\mu\nu}$

$$T^{\mu\nu} = \rho_0 u^\mu u^\nu + 2u^\mu q^\nu + t^{\mu\nu}, \tag{4.23}$$

where u^μ is the particle's 4-velocity, an energy flow vector q^μ and a stress tensor $t^{\mu\nu}$ measured in the averaged rest frame such that $u_\mu q^\mu = 0$ and $u_\mu t^{\mu\nu} = 0$.

Let us define the average torque W_ϕ^r by vertically integrating $\left\langle t_\phi^r \right\rangle$:

$$W_\phi^r = \int_{-h}^{h} \left\langle t_\phi^r \right\rangle dz. \tag{4.24}$$

In order to derive the time-averaged radial structure of the AD, we need to consider the conservation of mass, energy $E^\mu = -T^\mu_\nu(\partial/\partial t)^\nu$ and angular momentum $J^\mu = T^\mu_\nu(\partial/\partial\phi)^\nu$,

just like we did for the Newtonian case.

Using Gauss's law, the time-averaged accretion rate $\dot{M}$ can be obtained from the conservation of rest mass $\nabla_\mu (\rho_0 u^\mu) = 0$

$$\dot{M} \equiv -2\pi\sqrt{-g}\Sigma u^r, \tag{4.25}$$

where u^r is the particle's radial velocity and $\sqrt{-g}$ is the metric determinant.

Integrating the energy conservation law $\nabla_\mu E^\mu = 0$ yields

$$\left[\dot{M}_0 E - 2\pi\sqrt{-g}\Omega W^r_\phi\right]_{,r} = 4\pi\sqrt{-g}\mathcal{F}E, \tag{4.26}$$

where $\mathcal{F}$ is the time-averaged flux of the disk. Equation (4.26) states that the energy radiated from the AD's surface $4\pi\sqrt{-g}\mathcal{F}E$ results of the balance between the rest-mass energy flow $\dot{M}_0 E$ and the work done by viscous stresses in the disk $2\pi\sqrt{-g}\Omega W^r_\phi$.

Integrating the angular momentum conservation law $\nabla_\mu J^\mu = 0$ yields

$$\left[\dot{M}_0 L - 2\pi r W^r_\phi\right]_{,r} = 4\pi\sqrt{-g}\mathcal{F}L. \tag{4.27}$$

Similarly, the first term in equation (4.27) represents the angular momentum carried by the rest mass flow in the disk and $2\pi r W^r_\phi$ represents the angular momentum transported by viscous torques in the disk. These terms are balanced by the angular momentum carried away from the disk's surface $4\pi\sqrt{-g}FL$.

In order obtain an expression for $\mathcal{F}$, we need to eliminate the viscous torques W^r_ϕ from equations (4.26) and (4.27) and to apply the circular orbit relation $E_{,r} = \Omega_\phi L_{,r}$. Finally, the radial flux of the AD yields

$$\mathcal{F}(r) = -\frac{\dot{M}_0}{4\pi\sqrt{-g}}\frac{\Omega_{,r}}{(E-\Omega L)^2}\int_{r_{in}}^{r}(E-\Omega L)L_{,r}dr. \tag{4.28}$$

Let also define the luminosity L of the disk which takes into account the entire flux distribution

$$\mathcal{L} = 4\pi\int_{r_{in}}^{\infty}\mathcal{F}(r)r dr. \tag{4.29}$$

Novikov-Thorne model is believed to be a good description of the accretion process when the disk luminosity is $\sim 30\%$ of the Eddington Luminosity. The model has been widely used in the literature for modeling BH candidates constituting X-ray binaries and AGNs. In fact, most X-ray spectroscopy models use it to describe the flow dynamics responsible for the emission spectra. The uncertainties introduced from this assumption have been constrained [63] and do not limit the accuracy of the results.

The derivation above does not limit the nature of the accreting compact object. Thus, the model can be adapted to different astrophysical objects, as is the case of NBSs, by incorporating their circular orbit behaviour.

4.3 Thorne limit

We are now going to understand how a Kerr BH changes during the accretion process. Our goal is to find explicit expressions for its mass M and spin a^* as a function of the accreted rest mass M_o. Bardeen [64] was the first physicist to perform this calculation for the first time in 1970. One of the main assumptions of his calculation was the neglection of AD's thermal photons accretion, considering that the only particles accreting to the BH were the ones plunging directly from r_{ISCO}.

Assuming a vacuum exists between the inner edge of the disk and the BH, we can neglect any losses that occur between ISCO and the BH. Thus, after completing the last stable circular orbit, matter will plunge directly into the BH carrying along an energy E_{ISCO} and an angular momentum L_{ISCO}, corresponding to their values on the last stable orbit.

Intuitively, we expect that as the BH accretes matter from the disk, M and a^* will increase. The inner edge of the disk r_{isco} will naturally compensate for these effects as it depends on the properties of spacetime, which is now changing due to accretion.

If a BH accretes a rest mass ΔM_0, its mass will change ΔM and its total angular momentum change ΔJ

$$\Delta M = E_{ISCO}(z)\Delta M_0 \quad \Delta J = L_{ISCO}(z)\Delta M_0, \tag{4.30}$$

where $z = r_{ISCO}/M$.

As Kerr spacetime depends only on the BH mass M and spin a, there is a direct relation between r_{ISCO} and a^*. Assuming circular equatorial and stable orbits, we can express E_{ISCO}, L_{ISCO} and a^* as a function of z and M:

$$E_{isco}(z) = \sqrt{1 - \frac{2}{3z}} \tag{4.31}$$

$$L_{isco}(z, M) = \frac{2M}{\sqrt{27}}[1 + 2\sqrt{3z - 2}] \tag{4.32}$$

$$a^*_{isco}(z) = \frac{1}{3}\sqrt{z}[4 - \sqrt{3z - 2}]. \tag{4.33}$$

The differential equation governing a^* evolution can be obtained using the chain rule, the definition of $a^* = J/M^2$ and (4.30):

$$\frac{da^*}{dM} = \frac{d(J/M^2)}{dM} = \frac{1}{M^2}\frac{L_{ISCO}}{E_{ISCO}} - \frac{2}{M}a^*. \tag{4.34}$$

Accretion increases (decreases) the BH spin if the right hand side of (4.34) is positive (negative). When the right hand side vanishes, the BH spin reaches the equilibrium value which depends on the spacetime solution considered.

We then rewrite (4.34) as a function of z derivatives:

$$M\frac{d\tilde{a}}{dz}\frac{dz}{dM} = \frac{1}{M}\frac{L_{ISCO}}{E_{ISCO}} - 2\tilde{a}. \tag{4.35}$$

To solve this differential equation we plug the expressions for $a^*(z)$ (4.33), $E_{ISCO}(z)$ (4.31)and $L_{ISCO}(z)$ (4.32) obtaining the solution

$$\frac{z}{z_1} = \left(\frac{M_1}{M}\right)^2, \tag{4.36}$$

where z_1 and M_1 are the values of z and M when the BH started accreting. Without loss of generality, let us consider an initially static BH described by the Schwarzchild metric such that $z_1 = 6$. We can then plug the solution (4.36) in (4.33) and obtain an evolution law for a^* as a function of the BH current M and initial M_1 masses:

$$a_*(M) = \begin{cases} \sqrt{\frac{2}{3}}\frac{M_1}{M}\left[4 - \sqrt{18\left(\frac{M_1}{M}\right)^2 - 2}\right]. & \text{if } M \leq \sqrt{6}M_1 \\ 1 & \text{if } M > \sqrt{6}M_1 \end{cases} \tag{4.37}$$

We will focus now on describing how the BH's mass M changes with the accretion of a rest mass M_0. Starting from equation (4.30) we obtain the differential equation:

$$\frac{dM}{dM_0} = E_{ISCO}(z). \tag{4.38}$$

Substituting the energy $E_{ISCO}(z)$ (4.31) in the previous equation, we obtain, after integrating it, the current mass of the BH M as a function of its initial mass M_1 and the accreted rest mass M_0:

$$\frac{M}{M_1} = 2\sqrt{2}\sin\left(\frac{M_0}{3M_1}\right) + \cos\left(\frac{M_0}{3M_1}\right). \tag{4.39}$$

Figure 4.1 represents the spin a^* evolution of an initially static BH a^* as a function of its mass M.

We observe from figure 4.1 that the BH spin changes rapidly at the beginning of the accretion process and stabilises for $a^* = 1$. This result would mean that a BH would be maximal spinning after the accretion of a rest mass $\Delta M_0 \approx 1.5M_1$, which corresponds to increasing the BH mass only by a factor of $\sqrt{6} \sim 2.4$. This result is inconsistent with the cosmic censorship conjecture as it admits that BHs would develop naked singularities after relatively short accretion.

In 1969, Thorne [65] discussed the evolution of the BH spin due to accretion, including the contribution of angular momentum carried by thermal photons emitted from the AD. Some photons carry an angular momentum parallel with the BH's rotation, spinning it up. On the other hand, photons carrying an angular momentum anti-parallel with BH's rotation will spin the BH down.

As the cross-section for photons carrying anti-parallel angular momentum is larger (see section 2.1), their accretion originates a torque that will decrease the BH's spin. Thorne rewrote equations (4.37) and (4.38) including the energy and angular momentum contributions of the absorbed photons, obtaining

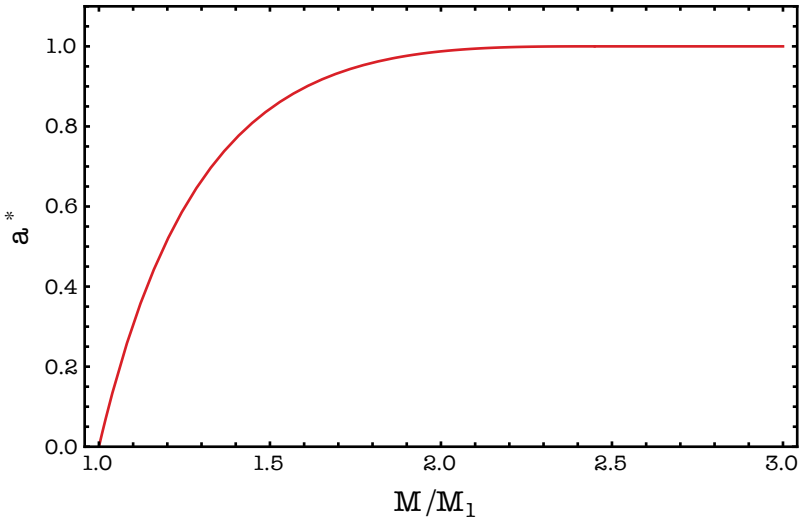

Figure 4.1: Spin evolution due to the accretion process for an initially static BH $a^* = 0$ as a function of its mass M.

$$\frac{da^*}{dM} = \frac{d\left(J/M^2\right)}{dM} = \frac{1}{M^2}\frac{L_{isco} + \dot{M}^{-1}(dJ/dt)_{\text{radiation}}}{E_{isco} + \dot{M}^{-1}(dM/dt)_{\text{radiation}}} - \frac{2}{M}a^* \tag{4.40}$$

and

$$\frac{dM}{dM_0} = E(z) + \dot{M}^{-1}(dM/dt)_{\text{radiation}}\ , \tag{4.41}$$

where $\dot{M}^{-1}(dJ/dt)_{\text{radiation}}$ and $\dot{M}^{-1}(dM/dt)_{\text{radiation}}$ are energy and the angular momentum contributions arising from photon's accretion.

Thorne numerically integrated the differential equations (4.40) and (4.41) and obtained a limit for the BH spin of $a^* \approx 0.998$, this result is known in the literature as Thorne limit. Besides, Thorne showed that if the initial spin is greater than this limit, the photon's accretion will slow the BH down to Thorne limit, never violating the cosmic censorship conjecture. It is worth noting that Bardeen and Thorne models agree for smaller values of spin $a* < 0.9$, meaning that the photon's effect only becomes relevant for large values of spin.

4.4 X-ray spectroscopy

BHs are believed to be associated with the strongest sources of X-Rays in the sky. X-ray spectroscopy studies the BH's emission spectra, consisting of two techniques: the continuum fitting method and reflection X-ray spectroscopy.

The theory is a powerful tool for testing the Kerr nature of BH candidates and GR in the strong field regime. X-ray spectroscopy methods have been extensively used to measure the spin of BH candidates, constrain deviations from Kerr spacetime and find signatures of BH mimickers. They were formulated to describe emissions from ADs around Kerr BHs but have been generalised to other spacetime backgrounds.

4.4.1 The continuum fitting method

The continuum fitting method analyses the thermal component of a geometrically thin and optically thick AD. The model usually assumes the disk is well described by the Novikov-Thorne model such that the AD flux $\mathcal{F}$ is modeled by equation (4.28). We assume that the disk locally behaves as a black-body, in the sense that locally is at thermal equilibrium with a temperature depending on the BH's mass and the accretion rate.

The thermal spectrum is strongly dependent on r_{ISCO} location as most of the flux is emitted closer to the inner edge of the disk. The emission in the inner region of the disk peaks in the optical/UV band (1-100 eV) for supermassive BHs and the soft X-ray band (0.1-1 keV) for stellar mass BHs. However, the technique has only been used to measure the spin of stellar mass BHs as the UV radiation is strongly absorbed by dust in the interstellar medium, making it difficult to obtain accurate measures [46].

The fit of the thermal spectrum measures the radiative efficiency $\eta = 1 - E_{ISCO}$ of the AD, where E_{ISCO} is the specific energy of a test particle at the ISCO radius. Thus, the thermal spectrum from an AD around a Kerr BH could be indistinguishable from the one around another compact object as long as the radiative efficiencies are the same.

The model depends on 5 parameters: the BH accretion rate $\dot{M}$, the BH mass M, the BH spin a^*, the inclination angle i to the line of sight of a distant observer and their distance D. When relaxing the Kerr hypothesis, e.g., by including deformation parameters to account for deviations of Kerr spacetime, more parameters need to be added to the model. These parameters are strongly degenerate, to reduce this effect the model usually requires independent measures for $\dot{M}$, M, i and D. When doing this, the spin a^* and possible deviation parameters are estimated by the fit of the thermal spectrum.

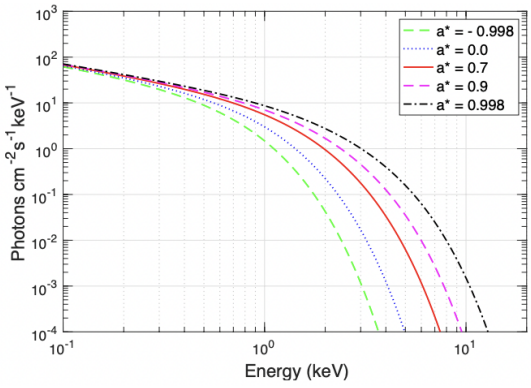

Figure 4.2: Numerical simulation of thermal spectrum for different values of the BH spin a^*. D=10kpc, $i = 45^o$, $M = 10M_\odot$ and $\dot{M} = 2 \times 10^{18} g/s$ (fig 1.8 in [1])

The high-energy cut-off on the thermal spectrum strongly depends on η. Thus, when considering a Kerr background, there is a direct relation between E_{ISCO} and a^*, allowing us to easily measure spins. Figure 4.2 shows the dependence of the high-energy cut-off on the BH spin.

4.4.2 Fe $K\alpha$ line method

The reflection X-ray spectroscopy, also known as the Fe K_α, is another method commonly used for measuring the spin of stellar mass and supermassive BH candidates and probe spacetime in the strong field regime.

The most standard approach is to consider a thin AD, described by the Novikov-Thorne model, surrounding a Kerr BH with a hotter and optically thin corona (100keV) located above it as represented in figure 4.3. The theory has been generalised to other compact objects such as neutron stars or boson stars.

Despite existing models describing the corona, its exact nature and geometry are still unknown. The most common choice for the corona's geometry is the lamp-post geometry, consisting of a point-like source aligned with the BH rotation axis.

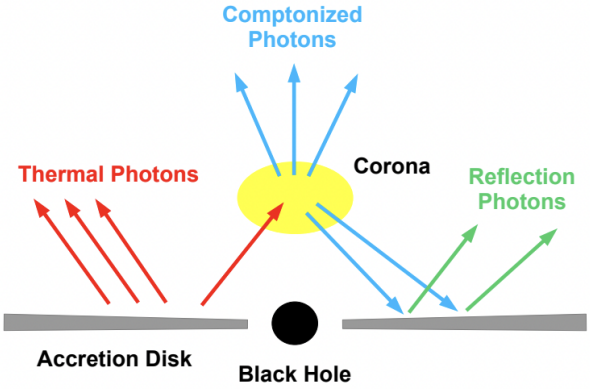

Figure 4.3: Schematic view of the disk-corona model including the AD, a corona and an accreting BH (fig.1 in [2])

The corona could be formed out of jets emitted from the BH, which did not have enough velocity to escape and were retained above the BH. Other models suggest the corona can be the atmosphere above the AD or matter plunging the BH from ISCO.

Thermal photons emitted closer to the disk's inner edge will inverse-Compton scatter off free electrons of the corona, originating an energetic X-ray continuum with power law cut-off. This power law component irradiates the colder AD with photons that are absorbed or suffer Compton scatter off electrons in the disk. The more energetic power-law photons are rarely absorbed, scattering back out of the disk and originating a broad hump peak at $20-30keV$. The result is a reflection component in the X-ray spectrum with some fluorescent lines. Due to its abundance, when compared with other elements in the disk, the fluorescent iron line - Fe $K\alpha$ - at $6.4keV$ is the strongest feature of the reflection spectrum [56].

The fluorescent lines form when an inner shell electron, K shell, is ejected due X-ray absorption of photons from the power law continuum component. Then, an electron from a higher shell drops into the K-shell, releasing energy and originating a fluorescent line at $6.4KeV$.

The line is intrinsically narrow in energy but gets skewed and asymmetric due to light

bending, Doppler boosting and gravitational redshift.

The shape of the line depends on the spacetime background metric, the geometry of the emitting region (mainly r_{ISCO} and some outer radius r_{out}), the disk's emissivity and the disk's inclination. Despite existing models for the disk's emissivity, the most straightforward approach is to consider it a free parameter to be determined by the fit.

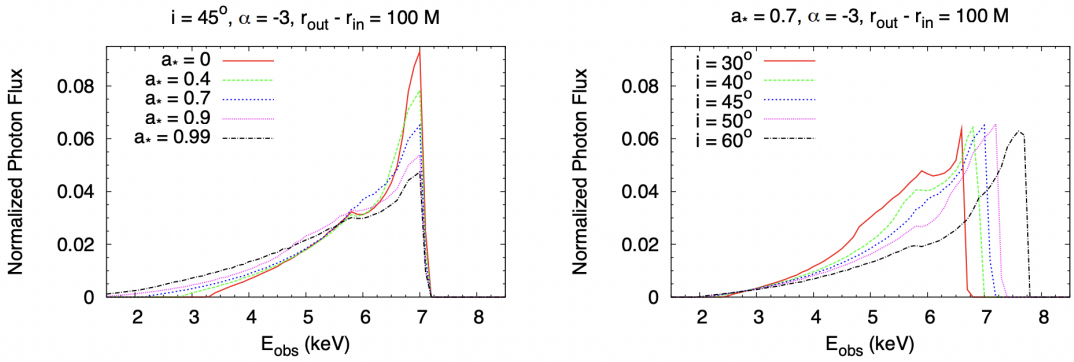

Figure 4.4: Numerical simulation of Fe line profiles for different model parameters. Left: The effect of the BH's spin a^* for an inclination of $i = 45^o$ and an emissivity region with a width of $r_{out} - r_{in} = 100M$. Right: The effect of the inclination of the disk $i = 45^o$ for a BH's spin of $a^* = 0.7$ and an emissivity region with a width of $r_{out} - r_{in} = 100M$. (Fig. 2 in [3])

The dependence of the Fe line on these parameters is well studied. Figure 4.4 represents how the line profile changes as a function of the inclination i and spin a^*. We verify that increasing the inclination parameter broadens the line, increasing its high-energy extent, which is mainly conditioned by the disk's inclination. On the other hand, the low-energy extent of the line strongly depends on the position of the inner radius of the emitting region. This happens as the red extent is mainly originated from the gravitational redshift in the inner region of the disk. Increasing a^* pushes the r_{ISCO} closer to the BH, resulting in a broader line with a longer low-energy tail.

Chapter 5

Newtonian boson stars as black hole mimickers

In this chapter, we will discuss the properties and observational signatures of ADs around BHs and NBSs. Then, we search for a parameter space of mass M and spin a^* such that NBS and BH disks have the same bolometric luminosities. Additionally, we compare if the study of the disk emission spectra can provide some insight into the nature of the accreting object. In conclusion, we analyse how well the models describe known supermassive BH candidates.

5.1 AD flux profiles

We are interested in comparing the properties of ADs around BHs with the ones of ADs around NBS with the same mass M. In the weak field limit, the boson field Ψ and the gravitational potential should be weak, verifying $|\Psi| \ll 1$ and $|\mathcal{U}| \ll 1$, respectively. This restricts both the M and the field's mass μ considered $\mu M \leq 0.55$.

We assumed a steady, geometrically thin and optically thick AD surrounding the central compact object, such that its flux $\mathcal{F}$ is well described by the Novikov-Thorne model (4.28). The inner edge of a disk around a Kerr BH is assumed to be at the ISCO radius $r = r_{ISCO}$ (2.17), while an AD around a NBS extends to $r = 0$. As discussed in section 3, this happens since spacetime around a NBS is always regular and circular stable orbits can be found for all radii.

We start by numerically computing $\mathcal{F}$ for an AD around a Schwarzchild BH ($a^* = 0$) $\mathcal{F}_{BH}$ and for an AD around an equally massive NBS $\mathcal{F}_{NBS}$. The results are depicted in figure 5.1. The two flux profiles exhibit a distinct behaviour for inner radii and asymptotically converge for the outer regions of the disk. $\mathcal{F}_{BH}$ has a peak closer to its inner edge $r_{ISCO} = 6M$, rapidly decreasing and extinguishing at $r = 6M$ with a cutoff for smaller radii. On the other hand, $\mathcal{F}_{NBS}$ also peaks close to its centre but extends smoothly to $r = 0$. Thus, providing we have instruments with a good radial resolution, observations of the AD radial flux profile from the inner region of the disk can indicate the presence of an ISCO.

The $\mathcal{F}_{BH}$ profile peak location is related to its proximity to r_{ISCO}, this happens as the model assumes that the viscous stresses, responsible for heating matter and making it making

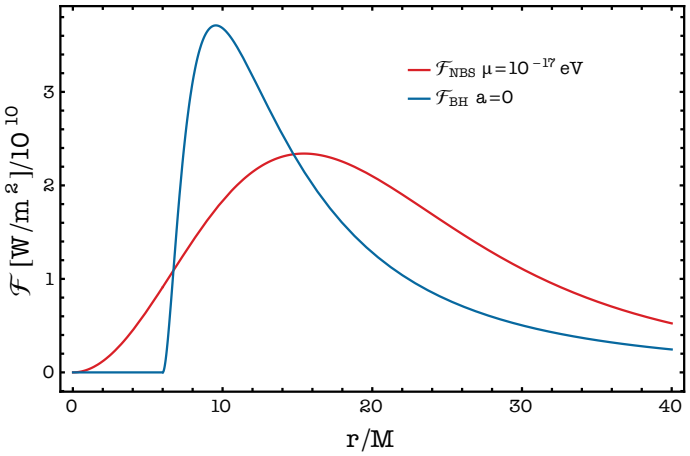

Figure 5.1: Radial flux profile of an AD around a Schwarzchild BH $\mathcal{F}_{BH}$ and a equally massive NBS $\mathcal{F}_{NBS}$ with $\mu = 10^{-17} eV$ and $M = 6.7 \times 10^6 M_\odot$.

radiate, vanish at its inner edge. The absence of an ISCO in the NBS spacetime suggests a different physical motivation is at the origin of the peak. Analysing all physical quantities on which the flux model depends, we concluded that the $\mathcal{F}_{NBS}$ peak is located extremely close to where the variation of the orbital velocity $\partial_r \Omega$ is maximal. This result agrees well with the Novikov-Thorne description of the disk dynamics as it is precisely the differential orbital angular velocity the base of the friction mechanism, responsible for thermal emission.

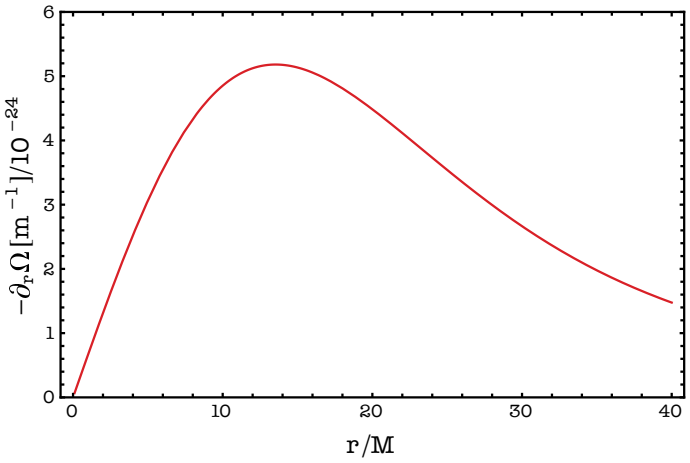

Figure 5.2: $-\partial_r \Omega_\phi$ for an AD around a NBS with $\mu = 10^{-17} eV$ and $M = 6.7 \times 10^6 M_\odot$.

However, $\mathcal{F}_{NBS}$ may be larger if one takes into account the energy radiated from the interaction between the disk particles and the NBS field, neglected in the Novikov-Thorne description.

5.2 AD flux dependencies

The AD flux strongly depends on the location of its inner edge, close to which the largest amount of radiation comes from, and on the properties of circular geodesic orbits of the surrounding spacetime, which are determined by the metric. The Kerr spacetime is completely described with the BH mass M and spin a^*, while the NBS spacetime only depends on its mass M and the boson field's mass μ.

To understand how $\mathcal{F}$ varies with the mass of the central object M, we numerically computed the AD flux for different M values for BHs and NBSs, the results are represented in figures 5.4 and 5.3, respectively.

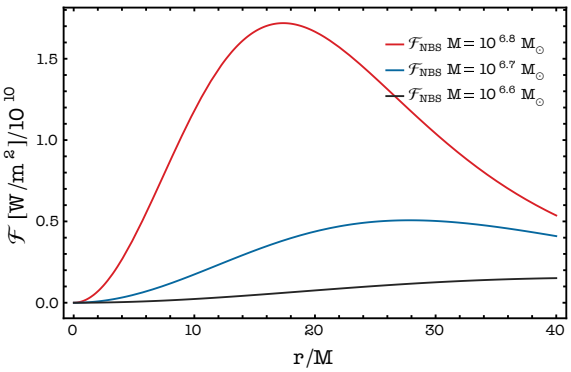

Figure 5.3: Radial flux profiles of ADs around NBS $\mathcal{F}_{NBS}$ with different M values and $\mu = 10^{-17} eV$.

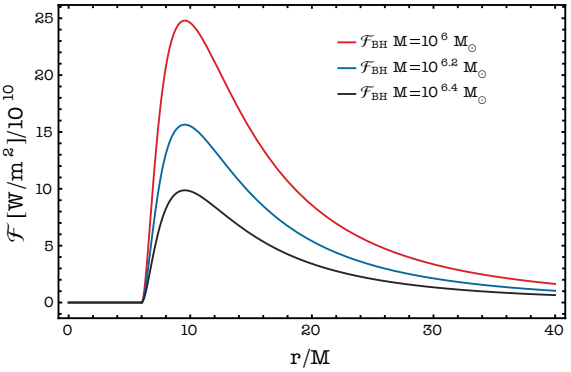

Figure 5.4: Radial flux profiles of ADs around Schwarzchild BHs $\mathcal{F}_{BH}$ with different M values.

We verify that $\mathcal{F}_{BH}$ decreases with the BH mass as $\mathcal{F}_{BH} \sim 1/M$. Let us now assume that matter in the disk locally behaves as a black-body with a temperature T, obeying the Stefan–Boltzmann law $\mathcal{F}_{BH} = \sigma T^4$. This mass dependency implies that ADs around stellar-mass BHs are hotter than the ones around supermassive BHs. Experimental observations from ADs around BH candidates have determined that the thermal radiation from ADs around supermassive BHs peaks for the optical/UV band, while the ones around stellar-mass BHs normally peak for more energetic frequency bands as the X-ray, corroborating this dependency.

The BH angular momentum determines the geometry of the disk by determining the location of its inner edge which is defined to be at r_{ISCO}. The Novikov-Thorne model relies on the Bardeen formula to establish the dependence of r_{ISCO} on the BH spin a^*. Figure 5.5, represents how the $\mathcal{F}_{BH}$ profile changes when varying the spin parameter a^*.

We verify that increasing a^* pushes the inner edge of the disk toward the BH, increasing the BH flux. This happens in part because the BH gravitational field is stronger for inner radii increasing the particle's orbiting angular velocity responsible for the shearing motion mechanism, making them radiate more. Besides, as we increase a^*, particles will complete more orbits before plunging the BH from r_{ISCO}, dissipating more potential energy as radiation.

NBSs have been widely discussed in the context of fuzzy DM models for massive fields of $\mu \sim 10^{-20} - 10^{-22} eV$ [61]. However, the mass spectrum of a boson field theory is yet

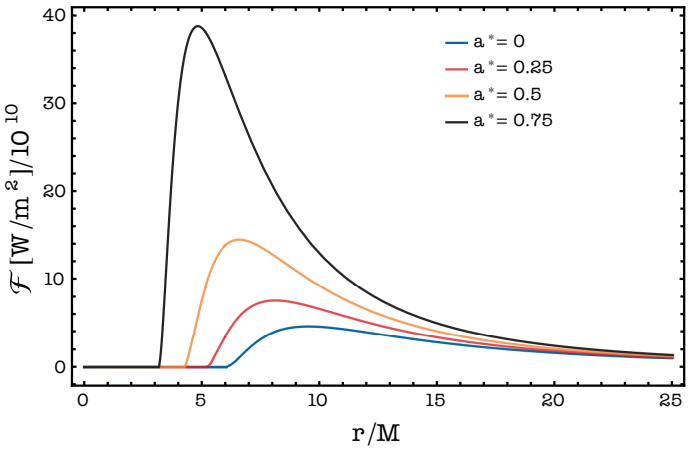

Figure 5.5: Radial flux profiles of ADs around Kerr BHs $\mathcal{F}_{BH}$ with $M = 5.3 \times 10^6 M_\odot$ for different a^* values.

to be determined and other mass values could be considered. To understand how μ affects $\mathcal{F}_{NBS}$, we numerically computed the AD flux for different μ values. The results are depicted in figure 5.7.

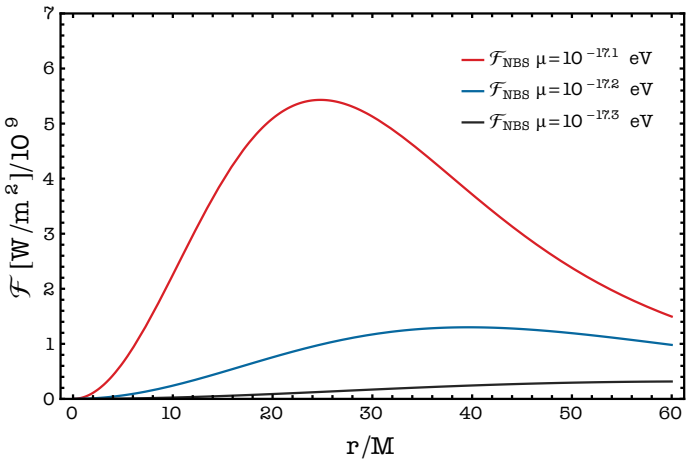

Figure 5.6: Radial flux profiles of ADs around NBSs $\mathcal{F}_{NBS}$ with $M = 6.7 \times 10^6 M_\odot$ for different field's mass μ values.

Analysing figure 5.7, we verify that $\mathcal{F}_{NBS}$ is very sensitive to small variations of μ, a small decrease of the field mass reduces the flux and moves its peak toward larger radii. This happens as decreasing μ dilutes the NBS spacetime solution, weakening the gravitational potential responsible for the disk accretion resulting in fainter radiation emission.

5.3 NBS as BH mimickers: a luminosity analysis

Current observational methods do not have enough angular resolution to solve an AD flux profile accurately. Thus, one usually analyses the total photon flux as a function of the energy. The bolometric luminosity $\mathcal{L}$ of the AD (4.29) is a measurable physical quantity which depends on the properties of the flux profile. Given the mass of the central compact object, obtained from different experimental methods, $\mathcal{L}$ may allow us to conclude about its nature.

Assuming that the central compact objects have the same mass M, if the luminosity of a disk around a BH $\mathcal{L}_{BH}$ is the same as the one of a NBS disk $\mathcal{L}_{NBS}$, their ADs could be harder to distinguish observably. We are now interested in finding a central mass M, a scalar field mass μ and a BH spin a^* parameters such that the luminosities of the BH and NBS disks are the same $\mathcal{L}_{NBS} = \mathcal{L}_{BH} = \mathcal{L}$.

Figure 5.7 represents the luminosity $\mathcal{L}$ for a NBS and a static BH as a function of μM.

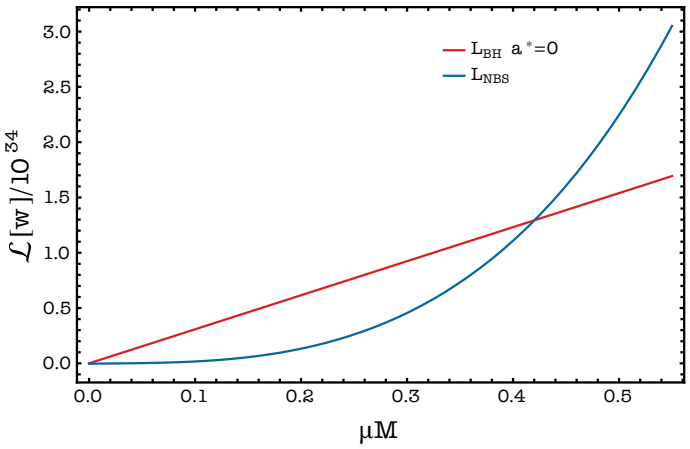

Figure 5.7: Luminosity curves for an AD around NBS $L_{NBS}/$ and a static BH L_{BH} as a function of μM.

We verify that as we increase the mass of the central compact object the disk's luminosity increases, $\mathcal{L}$ goes with M for the case of a BH (5.1) and with M^3 for a NBS (5.2).

$$\mathcal{L}_{BH} \sim 10^{34} \left(\frac{M}{4.3 \times 10^6 M_\odot} \right) [W] \tag{5.1}$$

$$\mathcal{L}_{NBS} \sim 6 \times 10^{33} \left(\frac{M}{4.3 \times 10^6 M_\odot} \right)^3 \left(\frac{\mu}{10^{-17} eV} \right)^2 [W] \tag{5.2}$$

Assuming the Novikov-Thorne model, an AD around a Schwarzchild BH has the same luminosity as an AD around a NBS for $\mu M \approx 0.42$ which corresponds to a central mass

$$M \sim 5.7 \times 10^6 \left(\frac{\mu}{10^{-17} eV} \right) M_\odot. \tag{5.3}$$

However, BH candidates are thought to be well described by Kerr's spacetime. Thus, a

more realistic approach needs to take the BH spin into account. As $\mathcal{L}_{BH}$ increases with spin a^*, the only possibility for having $\mathcal{L}_{BH} = \mathcal{L}_{NBS}$, while respecting the NBS regime constraints, is to restrict our analysis to the mass interval $0.42 \leq \mu M \leq 0.55$.

For each mass value μM in $0.42 \leq \mu M \leq 0.55$, we numerically computed $\mathcal{L}_{BH}$ and found the BH spin a^* such that $\mathcal{L}_{NBS}$, for an equally massive central object. Figure 5.8 represents a^* as a function of the central mass M such that $\mathcal{L}_{NBS} = \mathcal{L}_{BH}$.

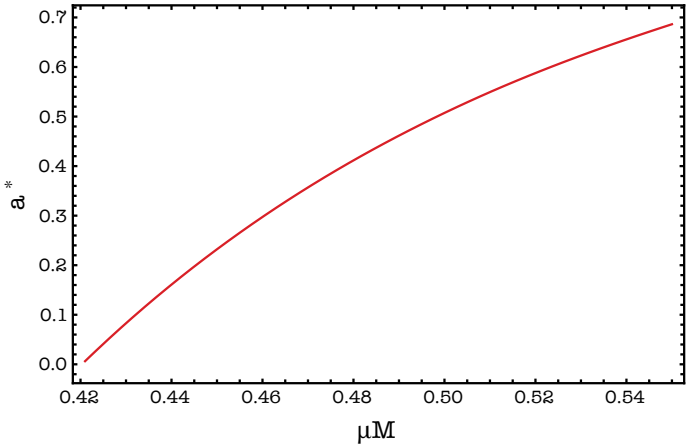

Figure 5.8: BH's spin as a function of μM such that the luminosity of an AD around a NBS is the same as an equally massive Kerr BH.

We conclude that for the mass values in $0.42 \leq \mu M \leq 0.55$ it was possible to find a Kerr BH such that the luminosities of the disks are the same. We verify that the greater the mass M of the central compact object the higher the spin a^*. The BH spin values obtained verify $a_* \leq 0.655$, which is compatible with the cosmic censorship conjecture and agrees well with some spin values obtained from X-ray spectroscopy [46].

Despite having the same bolometric luminosities, we have shown that the geometry and properties of ADs around BHs and NBSs are expected to be considerably different closer to the inner edge of the disk. To better understand these differences, we will now analyse the flux profiles of ADs around BHS and NBSs with the same mass M and the same bolometric luminosity $\mathcal{L}$, considering a static BH and a Kerr BH. Figure 5.9 represents $\mathcal{F}$ for the case of a static BH and a NBS with a mass of $M = 5.6 \times 10^6 M_\odot$. Figure 5.10 depicts $\mathcal{F}$ for $M = 7 \times 10^6 M_\odot$ and a BH's spin of $a^* \approx 0.6$.

The two profiles are completely distinguishable by the presence of the BH ISCO. We observe again that most of the BH disk emission occurs close to its inner edge while the flux for a NBS disk is smoother and dominates for larger radii. In fact, the peak of $\mathcal{F}_{BH}$ is 4 times larger than the one of $\mathcal{F}_{NBS}$, for the static BH, and 5 times larger, for the Kerr BH. The profiles converge asymptotically for the farthest regions of the disk. We also notice that for the cases considered, NBS disk emission for inner radii, i.e., smaller than BH r_{ISCO}, is considerably faint. This suggests that imaging of ADs may not be enough to conclude about their nature, especially when we take into consideration other effects such as light bending.

Assuming the black-body model applies locally in the disk, the temperature profiles would

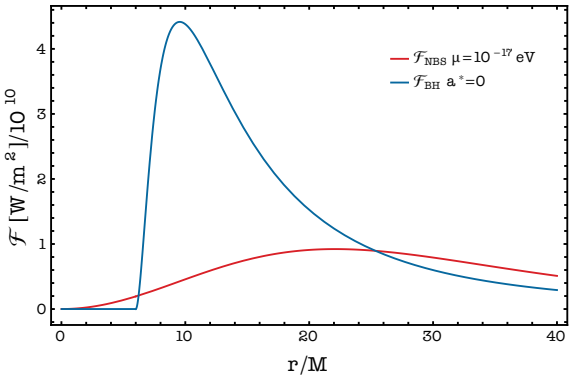

Figure 5.9: Flux profile $\mathcal{F}$ of an AD around a Schwarzchild BH $\mathcal{F}_{BH}$ and an equally massive NBS $\mathcal{F}_{NBS}$ with $\mu = 10^{-17} eV$ and $M = 5.6 \times 10^6 M_\odot$.

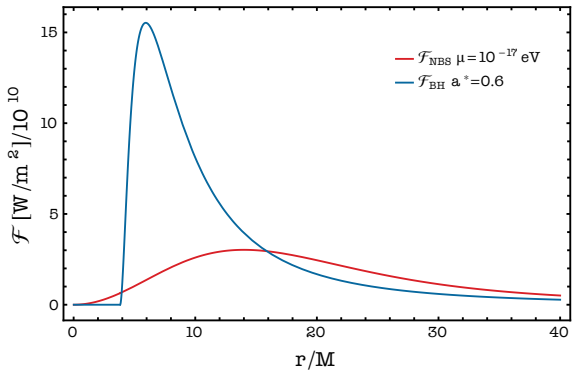

Figure 5.10: Flux profile $\mathcal{F}$ of an AD around a Kerr BH $\mathcal{F}_{BH}$ with $a^* = 0.6$ and around an equally massive NBS $\mathcal{F}_{NBS}$ with $\mu = 10^{-17} eV$ and $M = 7 \times 10^6 M_\odot$.

also be considerably different as a disk around a BH is expected to be much hotter than one around NBS. The temperature of the disk matter is a critical factor for thermal emission, determining which frequency bands dominate the flux. Thus, there could exist underlying signatures on the emission spectrum $\mathcal{L}(\nu)$ (4.18) even when the bolometric luminosity L is the same. This happens because $\mathcal{L}$ is computed by integrating energy flux from all different frequency bands, not differentiating band contributions. Figures 5.11 and 5.12 compare the emission spectrum of the disks for two cases considered.

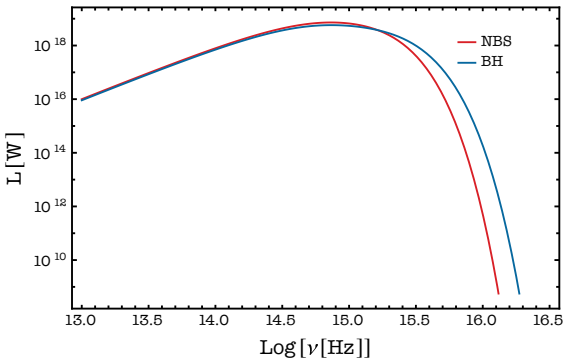

Figure 5.11: Emission spectra of an AD around a Schwarzchild BH and an equally massive NBS with $\mu = 10^{-17} eV$ and $M = 5.6 \times 10^6 M_\odot$.

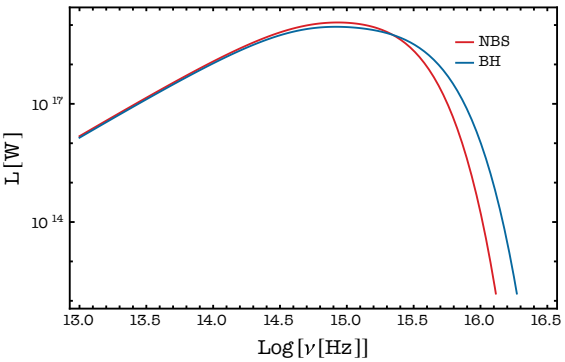

Figure 5.12: Emission spectra of an AD around a Kerr BH with $a^* = 0.6$ and around an equally massive NBS with $\mu = 10^{-17} eV$ and $M = 7 \times 10^6 M_\odot$.

We observe that the spectra look identical for lower frequencies and start to diverge for frequencies larger than $\nu \approx 10^{15} Hz$ (UV range). The spectra of a disk around a BH dominate for the highly energetic UV band, with some emission in the X-ray band. This happens because ADs around BHs get considerably hotter than the ones around NBSs. Thus, the disk spectra may be used to better understand the nature of accreting BH candidates as one expects a higher prominence for the most energetic bands for a Kerr background spacetime.

Figure 5.13 represents the disk spectra for different BH spin a^*. Given a central accreting mass M, increasing the BH's spin a^* shifts the high energy tail toward higher frequencies (more energetic UV/ X-ray). As the disk inner edge is pushed closer to the BH, particles need to lose more energy to reach those radii, increasing the flux from the hotter regions of the disk.

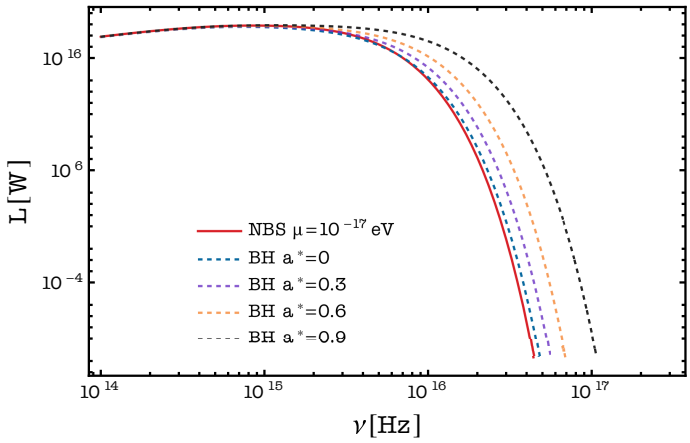

Figure 5.13: Emission spectra of disks around BHs with different spin values a^* and $M = 5.6 \times 10^6 M_\odot$ and the emission spectrum of an equally massive NBS with $\mu = 10^{-17} eV$.

X-ray spectroscopy could be crucial in determining whether the AD flux behaves considerably differently for NBSs and BHs for the inner regions of the disk, it would be interesting to consider the effects of both spacetime solutions when modeling Fe line profiles.

We will now briefly discuss how well NBS describe known supermassive BHs candidates, more precisely, AGNs. We are interested in finding which boson field mass μ needs to be considered to account for the observations. To achieve this, we will rely on measurements of the AGNs bolometric luminosities $\mathcal{L}_{obs}$ and of their mass M, usually inferred from observations of gas dynamics and nearby stars movement. Most of the time, $\mathcal{L}_{obs}$ needs to be approximated from the optical luminosity or the X-ray luminosity. This allows us to avoid problems related to the deficiency of frequency band coverage and data variability.

Using (5.2) and assuming $\mathcal{L}_{obs}$ has an associated uncertainty factor of 10 we compute a field mass interval μ which agrees with the observations. Table 5.1 presents the data related to the 4 AGNs considered, which are commonly used in the literature for calibration methods [66].

Object	$M/10^6 M_\odot$	$\mathcal{L}_{obs}[W]$	$\mu[eV]$
NGC 4151	45	$10^{33.3\pm1}$	$10^{-18} - 10^{-17}$
3C 120	55	$10^{35,48\pm1}$	$10^{-17} - 10^{-16}$
MRK 79	52	$10^{32\pm1}$	$10^{-19} - 10^{-18}$
M87	6500	$10^{34.18\pm1}$	$10^{-19} - 10^{-18}$

Table 5.1: AGN data: object name, mass M, observed luminosity $\mathcal{L}_{obs}$ and the field mass interval μ compatible with the NBS accretion dynamics (5.2)

The values of μ obtained sustain that light boson fields could potentially be used to describe supermassive BH candidates. However, we verify that the field mass spectrum compatible with the AGNs luminosities is considerably broad, ranging from $\mu = 10^{-16} eV$ to $\mu = 10^{-19} eV$. There is no single value of the scalar mass μ compatible with all observations.

Chapter 6

Conclusions

Understanding what happens in extreme gravity conditions such as the ones close to BHs is, ultimately, a test of the general relativity description of the universe. The pathological behaviour of gravity inside the BH horizon suggests that the Kerr solution may only be a grasp at the full explanation. The answer may include a quantum theory of gravity or undiscovered DM particles to be added to the standard model. Deepening our description of the intricate accretion phenomena for different compact objects helps us lift the veil and get one step closer to understanding the universe.

In this work, we studied if compact objects made out of light boson fields, as is the case of NBSs, could mimic the accretion of a Kerr BH for a geometrically thin disk described with the Novikov-Thorne model.

We numerically solved Poisson-Schrödinger equations for a self-gravitating object made of light boson fields to obtain the metric of NBS spacetime. We found a mass limit for the NBS mass compatible with the Newtonian approximation of $\mu M \leq 0.55$. We studied the properties of equatorial circular orbits for NBSs, concluding that stable orbital motion can always be found. These results were incorporated into the Novikov-Thorne model to describe NBS accretion dynamics.

We obtained flux profiles for NBSs, which are distinguishable from the ones of Kerr BHs due to the absence of an ISCO. Most of the emission of BH disks occurs close to the ISCO radius, while the NBS disk flux is smoother and extends for larger radii. Then, we discussed how the flux of an AD around a NBS peaks for the portion of the disk where particle differential rotation Ω_ϕ, required for viscous stresses, is higher. Furthermore, we analysed the flux dependence on the central object mass, BH spin and boson mass.

To compare the AD flux profiles for NBSs and equally massive BHs, we computed their luminosity as a function of μM and concluded that an NBS accretion flow could mimic the one of a Kerr BH for $0.4 \leq \mu M \leq 0.55$. Then, for each μM, we computed the BH spin such that the disk luminosities were the same and verified the values obtained $a^* < 0.66$ agree with the cosmic censorship conjecture. Finally, we compared the emission spectra of disks with the same luminosities for central masses of $\sim 10^6 M_\odot$. We verified that a NBS disk is colder than a BH one, emitting more weakly for the highly energetic UV/X-ray band. Thus, observations of disks emission for high frequencies may be used to assess the nature of the

accreting object.

Finally, we briefly discussed the boson field mass required to match the luminosity of a few AGNs. The mass interval obtained was quite extensive $\mu \sim 10^{-16} - 10^{-19} eV$. Our results suggest that NBSs could potentially be considered in describing some AGNs but there is no single boson field mass which could account for all supermassive BH candidates considered.

The AD emission profile differs considerably whether the accreting object is a Kerr BH or a NBS. Thus, the study of Fe K_α line profiles in X-ray spectroscopy, very sensitive to differences closer to the inner edge of the disks, could provide other observational signatures to distinguish NBS and BHs.

Bibliography

[1] C. Bambi, (2022), arXiv:2210.05322 [gr-qc] .

[2] C. Bambi, Arab. J. Math. **11**, 81 (2022), arXiv:2106.04084 [gr-qc] .

[3] C. Bambi, Phys. Rev. D **87**, 023007 (2013), arXiv:1211.2513 [gr-qc] .

[4] I. Newton, *Philosophiae naturalis principia mathematica ; Perpetuis commentariis illustrata, communi studio Thomae le Seur et Francisci Jacquier* (Duncan, 1822).

[5] A. Einstein, Annalen Phys. **17**, 891 (1905).

[6] A. Einstein, Annalen Phys. **49**, 769 (1916).

[7] J. Michell, Philosophical Transactions of the Royal Society of London **74**, 35 (1784).

[8] S. Chandrasekhar and E. A. Milne, Mon. Not. Roy. Astron. Soc. **91**, 456 (1931).

[9] F. Ozel, D. Psaltis, R. Narayan, and A. S. Villarreal, Astrophys. J. **757**, 55 (2012), arXiv:1201.1006 [astro-ph.HE] .

[10] J. R. Oppenheimer and H. Snyder, Phys. Rev. **56**, 455 (1939).

[11] K. Schwarzschild, Sitzungsber. Preuss. Akad. Wiss. Berlin (Math. Phys.) **1916**, 189 (1916), arXiv:physics/9905030 .

[12] D. Finkelstein, Phys. Rev. **110**, 965 (1958).

[13] R. P. Kerr, Phys. Rev. Lett. **11**, 237 (1963).

[14] W. Israel, Phys. Rev. **164**, 1776 (1967).

[15] B. Carter, Phys. Rev. Lett. **26**, 331 (1971).

[16] D. C. Robinson, Phys. Rev. Lett. **34**, 905 (1975).

[17] R. W. Romani, D. Kandel, A. V. Filippenko, T. G. Brink, and W. Zheng, Astrophys. J. Lett. **934**, L18 (2022), arXiv:2207.05124 [astro-ph.HE] .

[18] R. Narayan and J. E. McClintock, (2013), arXiv:1312.6698 [astro-ph.HE] .

[19] J. Kormendy and D. Richstone, Ann. Rev. Astron. Astrophys. **33**, 581 (1995).

[20] V. C. Rubin and W. K. Ford, Jr., Astrophys. J. **159**, 379 (1970).

[21] N. Aghanim *et al.* (Planck), Astron. Astrophys. **641**, A1 (2020), arXiv:1807.06205 [astro-ph.CO] .

[22] L. Wyrzykowski *et al.*, Mon. Not. Roy. Astron. Soc. **416**, 2949 (2011), arXiv:1106.2925 [astro-ph.GA] .

[23] R. D. Peccei, Lect. Notes Phys. **741**, 3 (2008), arXiv:hep-ph/0607268 .

[24] R. D. Peccei and H. R. Quinn, Phys. Rev. Lett. **38**, 1440 (1977).

[25] J. L. Feng, Ann. Rev. Astron. Astrophys. **48**, 495 (2010), arXiv:1003.0904 [astro-ph.CO] .

[26] J. P. S. Lemos and O. B. Zaslavskii, Phys. Rev. D **78**, 024040 (2008), arXiv:0806.0845 [gr-qc] .

[27] M. Visser and D. L. Wiltshire, Class. Quant. Grav. **21**, 1135 (2004), arXiv:gr-qc/0310107 .

[28] C. B. M. H. Chirenti and L. Rezzolla, Class. Quant. Grav. **24**, 4191 (2007), arXiv:0706.1513 [gr-qc] .

[29] A. Chamblin, S. W. Hawking, and H. S. Reall, Phys. Rev. D **61**, 065007 (2000), arXiv:hep-th/9909205 .

[30] D. J. Kaup, Phys. Rev. **172**, 1331 (1968).

[31] C. Bambi, *Black Holes: A Laboratory for Testing Strong Gravity* (2017).

[32] H.-a. Shinkai and S. A. Hayward, Phys. Rev. D **66**, 044005 (2002), arXiv:gr-qc/0205041 .

[33] F. S. N. Lobo, Class. Quant. Grav. **23**, 1525 (2006), arXiv:gr-qc/0508115 .

[34] M. Gleiser, Phys. Rev. D **38**, 2376 (1988), [Erratum: Phys.Rev.D 39, 1257 (1989)].

[35] P. Pani, E. Berti, V. Cardoso, Y. Chen, and R. Norte, Phys. Rev. D **81**, 084011 (2010), arXiv:1001.3031 [gr-qc] .

[36] V. Cardoso, S. Hopper, C. F. B. Macedo, C. Palenzuela, and P. Pani, Phys. Rev. D **94**, 084031 (2016), arXiv:1608.08637 [gr-qc] .

[37] F. S. Guzman, Phys. Rev. D **73**, 021501 (2006), arXiv:gr-qc/0512081 .

[38] T. Harko, Z. Kovacs, and F. S. N. Lobo, Class. Quant. Grav. **26**, 215006 (2009), arXiv:0905.1355 [gr-qc] .

[39] C. S. J. Pun, Z. Kovacs, and T. Harko, Phys. Rev. D **78**, 084015 (2008), arXiv:0809.1284 [gr-qc] .

[40] T. Harko, Z. Kovacs, and F. S. N. Lobo, Phys. Rev. D **79**, 064001 (2009), arXiv:0901.3926 [gr-qc] .

[41] J.-w. Lee and I.-g. Koh, Phys. Rev. D **53**, 2236 (1996), arXiv:hep-ph/9507385 .

[42] F. S. Guzman and J. M. Rueda-Becerril, Phys. Rev. D **80**, 084023 (2009), arXiv:1009.1250 [astro-ph.HE] .

[43] G. Aad *et al.* (ATLAS), Phys. Lett. B **716**, 1 (2012), arXiv:1207.7214 [hep-ex] .

[44] D. H. Weinberg, J. S. Bullock, F. Governato, R. Kuzio de Naray, and A. H. G. Peter, Proc. Nat. Acad. Sci. **112**, 12249 (2015), arXiv:1306.0913 [astro-ph.CO] .

[45] H. L. Shipman, **16**, 9 (1975).

[46] C. Bambi, Annalen Phys. **530**, 1700430 (2018), arXiv:1711.10256 [gr-qc] .

[47] B. P. Abbott *et al.* (LIGO Scientific, Virgo), Phys. Rev. Lett. **116**, 061102 (2016), arXiv:1602.03837 [gr-qc] .

[48] K. Akiyama *et al.* (Event Horizon Telescope), Astrophys. J. Lett. **875**, L1 (2019), arXiv:1906.11238 [astro-ph.GA] .

[49] K. Akiyama *et al.* (Event Horizon Telescope), Astrophys. J. Lett. **930**, L12 (2022).

[50] D. Lynden-Bell, Nature **223**, 690 (1969).

[51] N. I. Shakura and R. A. Sunyaev, Astron. Astrophys. **24**, 337 (1973).

[52] I. D. Novikov and K. S. Thorne, in *Les Houches Summer School of Theoretical Physics: Black Holes* (1973) pp. 343–550.

[53] D. N. Page and K. S. Thorne, Astrophys. J. **191**, 499 (1974).

[54] S. A. Balbus and J. F. Hawley, Astrophys. J. **376**, 214 (1991).

[55] C. Bambi, JCAP **08**, 055 (2013), arXiv:1305.5409 [gr-qc] .

[56] A. C. Fabian, K. Iwasawa, C. S. Reynolds, and A. J. Young, Publ. Astron. Soc. Pac. **112**, 1145 (2000), arXiv:astro-ph/0004366 .

[57] R. Penrose, Riv. Nuovo Cim. **1**, 252 (1969).

[58] J. M. Bardeen, W. H. Press, and S. A. Teukolsky, Astrophys. J. **178**, 347 (1972).

[59] G. H. Derrick, J. Math. Phys. **5**, 1252 (1964).

[60] L. Visinelli, Int. J. Mod. Phys. D **30**, 2130006 (2021), arXiv:2109.05481 [gr-qc] .

[61] L. Annulli, V. Cardoso, and R. Vicente, Phys. Rev. D **102**, 063022 (2020), arXiv:2009.00012 [gr-qc] .

[62] E. Barausse, V. Cardoso, and P. Pani, Phys. Rev. D **89**, 104059 (2014), arXiv:1404.7149 [gr-qc] .

[63] A. K. Kulkarni, R. F. Penna, R. V. Shcherbakov, J. F. Steiner, R. Narayan, A. Sadowski, Y. Zhu, J. E. McClintock, S. W. Davis, and J. C. McKinney, Mon. Not. Roy. Astron. Soc. **414**, 1183 (2011), arXiv:1102.0010 [astro-ph.HE] .

[64] J. M. Bardeen, Nature **226**, 64 (1970).

[65] K. S. Thorne, Astrophys. J. **191**, 507 (1974).

[66] C. Ünal, F. Pacucci, and A. Loeb, JCAP **05**, 007 (2021), arXiv:2012.12790 [hep-ph] .